Concentration of myelin debris-like myelin basic protein-immunoreactive particles in the distal (anterior)-most part of the myelinated region in the normal rat optic nerve

June KAWANO[1,2]

[1]Division of Morphological Sciences, Department of Neurology, Kagoshima University Graduate School of Medical and Dental Sciences, Kagoshima, 890-8544, Japan
[2]Laboratory for Neuroanatomy, Department of Neurology, Kagoshima University Graduate School of Medical and Dental Sciences, Kagoshima, 890-8544, Japan

Running Title: myelin debris-like particles in optic nerve

*Correspondence to:

June Kawano, M.D., Ph.D.
Division of Morphological Sciences, Department of Neurology,
Kagoshima University Graduate School of Medical and Dental Sciences,
35-1, Sakuragaoka 8-chome, Kagoshima, 890-8544, Japan
E-mail: kawanoj@m2.kufm.kagoshima-u.ac.jp
ORCID ID: 0009-0002-1730-6519

Grant sponsor: Kagoshima University
Grant Number: Annual fund

Main points
· Concentration of myelin basic protein-immunoreactive particles is observed in the distal (anterior)-most part of the myelinated region in the normal rat optic nerve.
· These particles are visualized by fluorescent immunohistochemistry using mouse monoclonal anti-human myelin basic protein antibody (clone SMI-99).
· The myelin basic protein-immunoreactive particles in the normal rat optic nerve are morphologically similar to myelin debris in the damaged-optic nerve.
· These results suggest that the distal-most part is under mildly pathological condition.

KEY WORDS:
Myelin basic protein; Myelin debris; Rat optic nerve; Myelinated region; Immunohistochemistry

Abstract

In the myelinated region of the normal rat optic nerve, neuronal fibers are encircled by myelin sheaths except at nodes of Ranvier. In addition to these myelinated fibers, concentration of small particles was observed in the distal (anterior)-most part of the myelinated region. These particles were visualized by fluorescent immunohistochemistry using mouse monoclonal anti-human myelin basic protein (MBPh) antibody (clone SMI-99). Fluorescent double immunohistochemistry by using both the rat monoclonal anti-cow myelin basic protein (MBPc) antibody (clone 12) and the anti-MBPh antibody demonstrated that myelin basic protein immunoreactive-particles detected by the anti-MBPc antibody were almost completely overlapped with those immunostained by the anti-MBPh antibody. Since these antibodies have different target sites, these particles contained the real myelin basic protein. We hypothesized that the MBPh-immunoreactive particles were myelin debris-like structures in the normal rat optic nerve. Quantitative morphological analyses indicated that only 2 out of 6 differences in sizes and shape descriptors between the particles and myelin debris observed in the damaged-optic nerve were statistically significant. Glial fibrillary acidic protein-immunoreactivity and glutamine synthetase-immunoreactivity were seen in the particles. Majority of the particles were isolated from ionized calcium binding adapter molecule 1-labeled microglia. These results demonstrate that the myelin debris-like MBPh-immunoreactive particles are concentrated on the distal-most part of the myelinated region. This evidence suggests that the distal-most part is under mildly pathological condition. Furthermore, the evidence may provide clues as to the pathophysiological background that induces localized vulnerability of the myelin sheaths.

(241 words)

1 | INTRODUCTION

In the myelinated region of the normal rat optic nerve, neuronal fibers are encircled by myelin sheaths except at nodes of Ranvier (Black et al., 1985; Peters et al., 1991; Kawano, 2015b). The modal diameter of the myelinated axon is 0.9 µm, and the modal diameter excluding the myelin sheath is 0.7 µm (Forrester and Peters, 1967). Mean myelin thickness of large axons is 0.12 µm, and that of small axons is 0.08 µm (Melo et al., 2006). Individual oligodendrocytes provide, on average, 16 near axons with single myelin segments about 200 µm in length (Butt and Ransom, 1993). In myelin biochemistry, the main constituents of myelin are lipids (70% of its dry weight) and proteins (30% of the dry weight). The major central nervous system myelin proteins are proteolipid protein (PLP, 50% of myelin protein) and myelin basic protein (MBP, 30% of myelin protein; Chrast et al., 2011; Butt, 2013; Duncan and Radcliff, 2016). In the present study, concentration of small particles was observed in the distal (anterior)-most part of the myelinated region. These particles were visualized by fluorescent immunohistochemistry using mouse monoclonal anti-human myelin basic protein (MBPh) antibody (clone SMI-99) as a primary antibody. Since these particles morphologically resembled myelin debris distributed in the neural injury site, we hypothesized that the MBPh-immunoreactive particles were myelin debris-like structures in the normal rat optic nerve.

Myelin debris is produced by the breakdown of the myelin sheath immediately after neural injury. Myelin debris persists in the injury site and contributes to regeneration failure since myelin debris contains molecules that potently inhibit axon regeneration (Chen et al., 2000; Filbin, 2003) and remyelination (Kotter et al., 2006; Syed et al., 2016). Moreover, myelin debris mediates a persistent inflammatory response during injury progression (Jeon et al., 2008; Sun et al., 2010; Wang et al., 2015; Zhou et al., 2019). Recently, mildly pathological condition is demonstrated in the distal-most part. In this part, concentrations of

GFAP (glial fibrillary acidic protein) and GS (glutamine synthetase) have been shown (Kawano, 2025). The concentration of GFAP suggests astrogliosis, which is a secondary event to damage in the central nervous system (Messam et al., 2002). A significant increase in GS immunoreactivity of GS-immunoreactive cells indicates a chronic pathological condition (Ben Haim et al., 2021; Kawano, 2025). Thus, this evidence supports the hypothesis that the MBPh-immunoreactive particles were myelin debris-like structures in the normal rat optic nerve.

Here we show, by using immunohistochemical analyses, 1) the concentration of the MBPh-immunoreactive particles in the distal-most part of the myelinated region, 2) the MBPh-immunoreactive particles containing the real myelin basic protein, 3) the particles colocalizing with marker proteins for both neurons and glial cells, 4) the particles being engulfed by microglia; 5) morphological similarity between the particles and MBPh-immunoreactive myelin debris, and 6) distribution of the MBPh-immunoreactive particles in the distal-most part of the myelinated region in both the mouse and monkey optic nerves. Finally, based on these facts we suggest the followings. First, the concentration of the particles indicates that the distal-most part is under mildly pathological condition. Second, the concentration of the particles may provide clues as to the pathophysiological background that induces localized vulnerability of the myelin sheaths. Lastly, MBPh-immunoreactive particles and/or myelin debris can be used as histopathological biomarkers.

2 | MATERIALS AND METHODS

2.1 | Animals and tissue preparation

2.1.1 | Normal rats and mice

Male rats (n=13; 12 weeks old; Slc:SD; CLEA Japan, Tokyo, Japan) and male mice (n=3; 8 weeks old; C57BL/6NCrlCrlj; Charles River Laboratories Japan, Yokohama, Kanagawa, Japan) were used in this study. The animals were deeply anesthetized with sodium pentobarbital (50 mg/kg, i.p.), and perfused transcardially with 4 % paraformaldehyde dissolved in 0.1 M sodium phosphate buffer (PB; pH 7.4) at 4°C. The eyeballs including the optic nerve were removed from the skull, stored in the same fixative for 48 hours, and then immersed in 30 % saccharose in 0.1 M PB at 4°C until they sank. The eyeballs including the optic nerve were frozen in powdered dry ice, and sectioned in the meridian plane at a thickness of 25 µm on a cryostat. Sections were collected in a cryoprotectant medium (Warr et al., 1981; 33.3% saccharose, 1% polyvinylpyrrolidone (K-30), and 33.3% ethylene glycol in 0.067M sodium phosphate buffer (pH 7.4) containing 0.067% sodium azide) and stored at –30 °C prior to use (Kawano et al., 2008; Kawano, 2015b).

2.1.2 | Normal monkeys

The monkey eyeballs including the optic nerve were provided by Dr. Shiro Nakagawa (Professor Emeritus, Kagoshima University Graduate School of Medical and Dental Sciences). Male monkeys (n=2; adult; weighing 11.8 to 12.5 kg; *Macaca fuscata*) were initially anesthetized with ketamine hydrochloride (5 mg/kg, i.m.), followed by sodium pentobarbital (40 mg/kg, i.p.). Under deep anesthesia, the monkeys were flushed transcardially with heparinized physiological saline (1,000 units heparin/L), subsequently perfused with 4 % paraformaldehyde dissolved in 0.1 M PB containing 0.2% picric acid at

4°C (Nakagawa, personal communication). The eyeballs including the optic nerve were removed from the skull, stored in 4% paraformaldehyde in 0.1M PB without picric acid for 7 to 9 days, and then immersed in 30 % sucrose in 0.1 M PB at 4°C until they sank. The eyeballs including the optic nerve were frozen in powdered dry ice, and sectioned in the meridian plane at a thickness of 40 μm on a freezing microtome. Sections were collected in the cryoprotectant medium and stored at –30 °C prior to use (Kawano, 2015a).

2.1.3 | Experimental glaucoma model in the rat induced by episcleral vein cauterization (EVC)

Male rats (n=17; 12 weeks old; Slc:SD; CLEA Japan, Tokyo, Japan) were used in this study. All animals were housed in the Kagoshima University animal facility (Kagoshima University, The Center for Advanced Science Research and promotion, Division of Laboratory Animal Resources and Research) with ad libitum access to food and water under a 12-hour light/12-hour dark cycle at room temperature (23 ± 1 °C) and humidity (55 %). Induction of elevated intraocular pressure by EVC was performed on left eyes essentially according to a method developed by Shareef et al. (1995), since the method was followed by Kanamori et al. (2004) and by their research group (Naka et al., 2010). The rats were anesthetized by intraperitoneal injection of ketamine hydrochloride (100 mg/kg) and xylazine hydrochloride (10 mg/kg). After minimal conjunctival incision, four episcleral veins near the superior, temporal, and inferior rectus muscles were cauterized by diathermy using bipolar cautery forceps. The eyes were flushed with saline and treated with antibiotic ointment (Gentamicin Sulfate ointment; 1mg/g).

After induction of anesthesia with 2.0 % isoflurane in oxygen (2 L/min) delivered to an induction chamber, ketamine hydrochloride (60 mg/kg) and xylazine hydrochloride (6 mg/kg) were intraperitoneally injected. Intraocular pressures (IOPs) were measured in both

eyes of anesthetized rats using a rebound tonometer (TonoLab TV02; Icare Finland Oy, Vantaa, Finland) as described by Naka et al. (2010). The instrument was clamped to a ring stand with the probe oriented horizontally. Rats that placed on an adjustable table were positioned, and the height of the table was adjusted to locate the probe tip at the center of the cornea at 2-mm distance. In each recording session, the tonometer took six measurements judged reliable by internal software that eliminated the highest and lowest readings and then generated and displayed a mean IOPs; this was defined as the IOP at the specific time point (Naka et al., 2010).

At 2 weeks and 4 weeks after EVC, tissue preparation procedures in the glaucoma rats were the same as those in the normal rats and mice (2.1.1 ｜ Normal rats and mice).

All animal experiments were approved by the Institutional Animal Care and Use Committee of Kagoshima University (rats: MD11112, MD15029, MD18058; mice: MD07068; monkeys: 00205, 00445; glaucoma rats: MD15081, MD18045), and were conducted according to the related guidelines and applicable laws in Japan.

2.2 ｜ Antibody characterization

Please see TABLE 1 for a list of all primary antibodies used. These antibodies are listed in the “Journal of Comparative Neurology antibody database (Version 14)” except for the rabbit anti-glutamine synthetase (GS) antibody.

Glial fibrillary acidic protein (GFAP) The affinity purified anti-GFAP rabbit antibody (Dako, Glostrup, Denmark) recognizes a single protein band of ≈ 50 kDa in extracts from the mouse retina (Smith et al, 1997; Gaillard et al., 2008). Astrocytes were immunolabeled with this antibody against GFAP in the human optic nerve head (Ye and Hernandez, 1995). The staining obtained with this anti-GFAP antibody in the rat was similar to published results on the rat (Saari et al., 1997; Morcos and Chang-Ling, 2000; Ju et al.,

2005; Chang et al., 2007; Kawano, 2015b).

Glutamine synthetase (GS) The rabbit anti-GS antibody (Sigma-Aldrich, Saint Louis, MO) recognizes a single protein band of 45 kDa in extracts from the rat brain. The staining of GS in immunoblotting is specifically inhibited with the GS immunizing peptide (amino acids 357-373 with N-terminally added lysine). This amino acid sequence is identical in human, bovine, rat, hamster, and pig GS, and is highly conserved in chicken GS (single amino acid substitution; manufacturer's technical information). Müller cells in the retina and glial cells in the optic nerve are labeled with this antibody against GS (Riepe et al., 1977). The staining obtained with the this antibody in the rat was similar to that previously reported in the mouse (Haverkamp and Wässle, 2000; Hojo et al., 2000; Kawano et al., 2008) and rat (Riepe et al., 1977; Zabouri et al., 2011; Kawano, 2015b).

Ionized calcium binding adaptor molecule 1 (Iba1) Microglia and macrophages are immunostained with the rabbit polyclonal antibody against Iba1 (Wako, Osaka, Japan), however neurons and astrocytes are not immunoreacted with this antibody (Ito et al., 2001; manufacturer's technical information). The Iba1 antibody recognizes a single protein band of 17 kDa corresponding to the Iba1 protein in extracts from rat brain microglia cultures and from several human monocytic cell lines (Imai et al., 1996). This antibody stains retinal and optic nerve microglia in the mouse (Bosco et al., 2008; Santos et al, 2008; Bosco et al., 2011) and in the rat (Naskar et al., 2002; Johnson et al., 2007; Zhang et al., 2009). The staining obtained with this antibody against Iba1 was similar to that previously reported in the rat (Zhang et al., 2009).

Myelin basic protein, cow (MBPc) The rat monoclonal antibody against full length of the cow myelin basic protein (clone 12; Abcam, Cambridge, United Kingdom) recognizes 2 protein bands of 19 and 26 kDa on immunoblots of mouse brain tissue lysate (manufacturer’s technical information). This antibody stains myelin sheaths of cultured

oligodendrocyte precursor cells obtained from the postnatal day 7 rat brain (Dugas et al., 2006). The staining obtained with this antibody against the cow myelin basic protein was similar to that previously reported in the rat (Morcos and Chang-Ling, 2000).

Myelin basic protein, human (MBPh) The mouse monoclonal antibody against the human myelin basic protein (clone SMI-99; Covance, Princeton, NJ) detects 4 bands between 14 and 21 kDa, corresponding to 4 myelin basic protein (MBP) isoforms on immunoblots of the mouse cerebellum (Dyer et al., 1996; Talos et al., 2006). The SMI-99 antibody detects MBP from most mammalian species. The pig and chicken MBP do not react and the guinea pig MBP has slight reactivity. This antibody does not react with the 14kDa form of the rat MBP. The SMI-99 antibody detects the developing and adult myelin, and distinguishes oligodendrocytes from astrocytes, microglia, neurons and other cells in brain sections (manufacturer's technical information). The staining obtained with this antibody against the human myelin basic protein was similar to that previously reported in the rat (Morcos and Chang-Ling, 2000), except for the concentration of the MBPh-immunoreactive particles.

Neurofilament 200-kDa heavy chain (neurofilament 200) The polyclonal anti-neurofilament 200 antibody (Sigma-Aldrich, Saint Lois, MO) recognizes a single protein band of 200 kDa in extracts from the rat brain cytosolic S1 fraction (manufacturer’s technical information) and in those from the mouse brain (Benvegnù et al., 2010). The antibody shows wide species cross reactivity (manufacturer’s technical information). The staining obtained with this antibody against neurofilament 200 was similar to published results on the mouse (Howell et al., 2007) and rat (Naka et al., 2010; Kawano, 2015b).

2.3 Immunohistochemistry

Sections were processed using double-label immunohistochemistry as previously

described (Kawano et al., 2008; Kawano, 2015b) except for detecting MBP by using the rat monoclonal anti-MBPc antibody. Free-floating sections were pre-incubated for 2 hours with a 10% NGS blocking solution at 4 °C, and were then immunoreacted for 4 days with a mixture of rabbit and mouse primary antibodies in a 10% normal goat serum (NGS) blocking solution at 4 °C (TABLE 1). After two rinses for 10 minutes in 0.02M phosphate buffered saline (PBS) containing 0.3% Triton X-100 (PBST), the sections were incubated with a mixture of two secondary antibodies in PBS containing 5% NGS and 0.3% Triton X-100 for 24 hours at 4 °C. The two secondary antibodies used were Alexa Fluor 488 conjugated with the $F(ab')_2$ fragment of goat anti-rabbit IgG (H+L) (1:200; Molecular Probes, Eugene, OR) and Alexa Fluor 594 conjugated to the $F(ab')_2$ fragment of goat anti-mouse IgG (H+L) (1:200; Molecular Probes). The sections were washed once for 10 minutes in PBST, and then twice in PBS. The sections were mounted onto hydrophilic silanized slides (Dako Japan, Tokyo, Japan) in an equal-parts mixture of a 0.6% gelatin solution and PBS. After being air-dried, the sections were subjected to nuclear staining by using a bisBenzimide (bBM; Hoechst 33258, Sigma-Aldrich; 0.1 mg/ml) solution, and coverslipped with VECTASHIELD mounting medium (Vector Laboratories, Burlingame, CA).

In case of double-label immunohistochemistry by using the rabbit polyclonal anti-GS antibody and the rat monoclonal anti-MBPc antibody as primary antibodies, Alexa Fluor 488 conjugated with the $F(ab')_2$ fragment of goat anti-rabbit IgG (H+L) (1:500; Molecular Probes) and Alexa Fluor 594 conjugated to goat anti-rat IgG (H+L) preadsorbed (1:200; Abcam) were used as secondary antibodies.

In case of double-label immunohistochemistry by using the rat monoclonal anti-MBPc antibody and the mouse monoclonal anti-MBPh antibody as primary antibodies, Alexa Fluor 488 conjugated to goat anti-rat IgG (H+L) cross-adsorbed (1:500; Thermo Fisher Scientific, Waltham, MA) and Alexa Fluor 594 conjugated to goat anti-mouse IgG (H+L)

highly cross-adsorbed (1:500; Thermo Fisher Scientific) were used as secondary antibodies. Since Alexa Fluor 594 conjugated to goat anti-mouse IgG (H+L) highly cross-adsorbed slightly immunoreacted with the rat monoclonal anti-MBPc antibody, primary antibodies were not applied simultaneously but serially as follows. After 2 hours preincubation with the 10% NGS blocking solution, free floating sections were incubated 1 overnight with the mouse monoclonal anti-MBPh antibody. After two rinses in PBST, the sections were immunoreacted 3 hours with Alexa Fluor 594 conjugated to goat anti-mouse IgG (H+L) highly cross-adsorbed. After two washes in PBST, the sections were incubated 1 overnight with the rat monoclonal anti-MBPc antibody. After two rinses in PBST, the sections were immunoreacted 3 hours with Alexa Fluor 488 conjugated to goat anti-rat IgG (H+L) cross-adsorbed. The following procedures were the same as described above.

In order to eliminate the possibility of any cross-reaction between the secondary and primary antibodies from the wrong species, one of the two primary antibodies was removed. No cross-reactivity was observed in these control experiments (SUPPLEMENTARY FIGURE 1).

In normal rat cases, each staining protocol was performed on a minimum of 3 optic nerves from 3 separate rats. GS/MBPh staining[1], MBPc/MBPh staining, and Iba1/MBPh staining protocols were done on 5 optic nerves from 5 separate rats each. GS/MBPc staining, MBPc control staining[2], MBPh control staining, NS200/MBPh staining, and GFAP/MBPh

---

[1] The GS/MBPh staining indicates double-label immunohistochemistry by using the rabbit polyclonal anti-GS antibody and the mouse monoclonal anti-MBPh antibody.

[2] The MBPc control staining shows double-label immunohistochemistry by using the 10% normal goat serum (NGS) blocking solution proper instead of the mouse monoclonal anti-MBPh antibody solution in the first step, then by using the rat monoclonal anti-MBPc antibody solution in the next step.

staining protocols were performed on 3 optic nerves from 3 separate rats each. In glaucoma rat cases, GS/MBPh staining protocol was done on a total of 11 optic nerves in the operated side and a total of 11 optic nerves in the non-operated side from 11 separate rats. In normal mouse cases, GS/MBPh staining protocol was performed on a total of 3 optic nerves from 3 separate mice. In normal monkey cases, GS/MBPh staining protocol was done on a total of 2 optic nerves from 2 separate monkeys.

2.4 | Photomicrographs

Fluorescent photomicrographs were taken with an LSM700 or an LSM900 confocal laser scanning microscopes (Carl Zeiss Jena GmbH, Jena, Germany) at the Joint Research Laboratory, Kagoshima University Graduate School of Medical and Dental Sciences (See, Figure Legends). Images were transferred to Adobe Photoshop CS5 (Adobe Systems, San Jose, CA). The brightness and contrast of images were adjusted. No other adjustment was made.

2.5 | Image Analysis

The quantitation of all images was performed using ImageJ2 (Version 2.9.0/1.53t; developed by Wayne Rasband, National Institute of Mental Health, Bethesda, MD, USA).

2.6 | Measurement of mean area, mean perimeter, and of mean shape descriptors of MBPh-immunoreactive particles

Area, perimeter, and shape descriptors of each MBPh-immunoreactive particle were measured in a trapezoid-like image which showed distribution of the particles in the distal-most part of the myelinated region. The bottom of the image was set at the border between the unmyelinated and myelinated regions. The longitudinal length of the image was 250 μm.

In order to cut the background off the measurement area, the boundaries of the myelinated regions were split along the pia mater.

For each image, the process performed by the ImageJ2 program included the following: (a) performing the Subtract Background function to remove smooth continuous background from the image (Rolling Ball Algorithm; Radius: 10.0 pixels); (b) doing the Median filter function to reduce noise in the image (Radius: 2.0 pixels); (c) performing the Mean filter function to smooth the image (Radius: 2.0 pixels); (d) establishing the threshold in order to binarize the image (Auto; Moments); (e) applying the watershed; (f) analyzing particles to obtain area, perimeter, and shape descriptors (Circularity; AR (aspect ratio); Roundness; Solidity) of each MBPh-immunoreactive particle, and to count MBPh-immunoreactive particles (size, 1.0 μm^2-infinity; circularity, 0.00-1.00; check “Clear results”, “Add to manager”, “Exclude on edges”, and “Include holes”).

Mean area, mean perimeter, and mean shape descriptors of MBPh-immunoreactive particles were manually calculated based on the outputs of the measurement processes described above.

2.7 | Measurement of density of MBPh-immunoreactive particles

Number of MBPh-immunoreactive particles were counted as described above (2.6). Area of the trapezoid-like image, in which the particles were distributed, was measured as follows. For each image, the process performed by the ImageJ2 program included the following: (a) setting the threshold 1-255 to binarize the image (Manual). (b) analyzing particles to measure area (size, 100 μm^2-infinity; circularity, 0.00-1.00; check “Clear results”, “Add to manager”, and “Include holes”). Density of MBPh-immunoreactive particles was manually calculated based on the number of the particles and on the area that the particles were distributed.

2.8 | Statistical Analysis

No statistical methods were used to predetermine group sample size. However, our group sample sizes were similar to previously published studies by our group and others (Melo et al., 2006; Balaratnasingam et al., 2009; Kawano, 2015b). All biological replicates (n) were derived at least three independent experiments. Unless otherwise specified, no data were excluded from analysis. Individual experiment values were shown on bar graphs or box and whisker plots. In the bar graphs, the bar edges indicate means, and whisker extend represents standard deviation of the distribution. In the box and whisker plots, the upper whisker indicates the maximum value and the lower one represents the minimum value. The thick horizontal line in the box shows the median. The upper and lower borders of the box indicate the interquartile range.

All statistical analyses were performed with EZR (Easy R; Version 1.55; Saitama Medical Center, Jichi Medical University, Saitama, Japan), which is a graphical user interface for R (Version 4.1.3; The R Foundation for Statistical Computing, Vienna, Austria). More precisely, it is a modified version of R commander (Version 2.7-2; Fox, 2017) designed to add statistical functions frequently used in biostatistics (Kanda, 2013). Data were analyzed by the Kolmogorov-Smirnov test for normal distribution, the Shapiro-Wilk normality test, the two-variances F-test for homogeneity of variance, the two-sample t-test, and by the Mann-Whitney U test. $P < 0.05$ was considered significant.

3 | RESULTS

3.1 | Distribution of MBPh-immunoreactive particles in the normal rat optic nerve

MBPh-immunoreactive particles were concentrated on the distal-most part of the myelinated region in the normal rat optic nerve (FIGURE 1A). However, small number of

MBPc-immunoreactive particles were detected in the similar part of the myelinated region (FIGURE 1B). Interestingly, majority of both MBPh-immunoreactive and MBPc-immunoreactive particles were distributed on MBP-immunoreactive myelinated nerve fibers (FIGURE 1A, B).

3.2 | The anti-MBPh antibody immunoreacted with the real myelin basic protein and the MBPh-immunoreactive particles contained the real myelin basic protein

Fluorescent double immunohistochemistry by using the anti-MBPh and anti-MBPc antibodies demonstrates that majority of MBPh-immunoreactive particles were also immunolabeled with the anti-MBPc antibody that target amino acid sequence was different from that of the anti-MBPh antibody (FIGURE 2D). These facts indicate that the anti-MBPh antibody was immunoreactive for the real myelin basic protein and that the MBPh-immunoreactive particles contained the real myelin basic protein (FIGURE 2D).

The control studies show that cross-immunoreactions were not detectable between the mouse monoclonal anti-MBPh antibody and the Alexa Fluor 488 conjugated goat anti-rat secondary antibody (SUPPLEMENTARY FIGURE 1C), or between the rat monoclonal anti-MBPc antibody and the Alexa Fluor 594 conjugated goat anti-mouse secondary antibody (SUPPLEMENT FIGURE 1J). These facts indicate that the fluorescent double immunohistochemistry by using the mouse monoclonal anti-MBPh antibody and the rat monoclonal anti-MBPc antibody was not artificial but real. Accordingly, MBPh and MBPc double-immunoreactive particles visualized in FIGURE 2D were not false positive but real.

3.3 | Colocalization of neural and glial proteins in the MBPh-immunoreactive particles

3.3.1 | Colocalization of GFAP (glial fibrillary acidic protein) in the MBPh-immunoreactive particles

Moderate GFAP-immunoreactivity was observed in the MBPh-immunoreactive particles (see GFAP-immunoreactivity in the particles pointed by the arrowheads in FIGURE 3A, 3B, and 3D).

3.3.2 | Colocalization of GS (glutamine synthetase) in the MBPh-immunoreactive particles

GS-immunoreactivity was clearly observed in the MBPh-immunoreactive particles (see GS-immunoreactivity in the particles pointed by the arrowheads in FIGURE 4A, 4B, and 4D).

3.3.3 | Colocalization of NF200 (neurofilament 200-kDa heavy chain; neurofilament 200) in the MBPh-immunoreactive particles

Moderately NF200-immunoreactive fibers were observed in the MBP-immunoreactive particles (see NF200-immunoreactive fibers in the particles pointed by the arrowheads in FIGURE 4E, 4F, and 4H).

3.3.4 | Distribution of Iba1 (ionized calcium binding adapter molecule 1)-labeled microglia, and of the MBPh-immunoreactive particles

Majority of MBPh-immunoreactive particles were isolated from Iba1-labeled microglia (FIGURE 5D). We observed at least five MBPh-immunoreactive particles had been engulfed in an Iba1-labeled microglia (FIGURE 5D inset).

3.4 | Neuroanatomical comparison between the MBPh-immunoreactive particles and MBPh-immunoreactive myelin debris

The size of MBPh-immunoreactive particles (FIGURES 6C-D, 7A-E) was broadly similar to that of MBPh-immunoreactive myelin debris (FIGURES 6A-B, 7F-H).

We next quantitatively compared mean sizes (area and perimeter) and mean shape descriptors (circularity, AR (aspect ratio), roundness, and solidity) of MBPh-immunoreactive particles in the normal rat (NR) optic nerve to those of MBPh-immunoreactive myelin debris in the damaged optic nerve of the glaucoma rat (GR; TABLE 2). The ratios of NR means to GR means were distributed between 0.971 and 1.029. Therefore, all differences in the sizes and the shape descriptors between the particles and the myelin debris were less than 3 percents.

Results of two-sample t-tests ($p < 0.05$; $n = 5$ in the normal rat, $n=3$ in the glaucoma rat) were as follows: mean area, $p = 0.773$; mean perimeter, $p = 0.508$; mean circularity, $p = 0.032$; mean AR (aspect ratio), $p = 0.115$. Results of Mann-Whitney *U* tests ($p < 0.05$; $n = 5$ in the normal rat, $n=3$ in the glaucoma rat) were as follows: mean roundness, $p = 0.036$; mean solidity, $p = 0.134$. Thus, p-values of both mean circulatory and mean roundness were less than 0.05. Accordingly, mean circularity and mean roundness of the MBPh-immunoreactive particles were significantly different from those of the MBPh-immunoreactive myelin debris. Therefore, only 2 out of 6 differences in the mean sizes and the mean shape descriptors between the particles and the myelin debris were statistically significant (FIGURE 8).

3.5 | Distribution of the MBPh-immunoreactive particles in the mouse and monkey optic nerves

Considerable number of MBPh-immunoreactive particles were distributed in the distal-most part of the myelinated region in the mouse optic nerve (FIGURE 9). In addition, reasonable number of MBPh-immunoreactive particles were distributed in the distal-most part of the retrolaminar region in the monkey optic nerve (FIGURE 10).

4 | DISCUSSION

4.1 | Summary of results

We demonstrated the concentration of MBPh-immunoreactive particles in the distal-most part of the myelinated region in the normal rat optic nerve. The MBPh-immunoreactive particles contained the real myelin basic protein. The particles colocalized with neural and glial marker proteins, such as the GFAP, GS, and NS200 proteins. Majority of MBPh-immunoreactive particles were distributed on myelinated nerve fibers in the optic nerve, and were isolated from Iba1-immunoreactive microglia. All differences in mean sizes (area and perimeter) and mean shape descriptors (circularity, AR (aspect ratio), roundness, and solidity) between the MBPh-immunoreactive particles and the MBPh-immunoreactive myelin debris in the damaged-optic nerve of the glaucoma rat were less than 3 percents. The mean circularity and mean roundness of the particles were significantly different from those of the myelin debris. Accordingly, only 2 out of 6 differences in the mean sizes (area and perimeter) and the mean shape descriptors (circularity AR, roundness, and solidity) between the particles and the myelin debris were statistically significant. MBPh-immunoreactive particles were also observed in the distal-most part of the myelinated region in the mouse and monkey optic nerves.

4.2 | The mouse anti-MBPh antibody (SMI-99)

4.2.1 | Specificity of the mouse anti-MBPh antibody (SMI-99)

The present study demonstrated the concentration of MBPh-immunoreactive particles in the distal-most part of the myelinated region in the normal rat optic nerve. As for this evidence, few reports have appeared. Therefore, there is a remote possibility that the particles were visualized by a false-positive immunoreaction. It is required to examine whether the anti-MBPh antibody detected the MBP proper or a protein other than the MBP.

This notion was verified by using the anti-MBPc antibody; the target sequence of the anti-MBPc antibody is different from that of the anti-MBPh antibody (Saper, 2005). As for immunohistochemistry of the MBPh-immunoreactive particles, the anti-MBPh antibody against Ala-Ser-Asp-Tyr-Lys-Ser (ASDYKS) in position 131-136 of the classic human myelin basic protein (MBPh) gave the same staining pattern as another anti-MBPc antibody against Asp-Glu-Asn-Pro-Val-Val (DENPVV) in position 82-87 of the full length protein of the cow myelin basic protein (MBPc; FIGURE 2). In addition, cross-reactions were not detectable between the mouse monoclonal anti-MBPh antibody and the Alexa Fluor 488 conjugated goat anti-rat secondary antibody (SUPPLEMENTARY FIGURE 1C), or between the rat monoclonal anti-MBPc antibody and the Alexa Fluor 594 conjugated goat anti-mouse secondary antibody (SUPPLEMENTARY FIGURE 1J). These facts indicate that the fluorescent double immunohistochemistry by using the mouse monoclonal anti-MBPh antibody and the rat monoclonal anti-MBPc antibody was not false-positive but real. Thus, the anti-MBPh antibody immunoreacted with the real MBP. Therefore, the MBPh-immunoreactive particles contained the real MBP.

4.2.2 | Detection of the MBPh-immunoreactive particles by using the mouse anti-MBPh antibody (SMI-99)

MBP-immunoreactivity of the MBPh-immunoreactive particles visualized by using the mouse anti-MBPh antibody (SMI-99) for primary antibody was equivalent to that visualized by using the rat anti-MBPc antibody (clone 12). However, MBP-immunoreactivity of myelinated nerve fibers in the rat optic nerve visualized by using the anti-MBPh antibody was weaker than that visualized by using the anti-MBPc antibody (FIGURE 1). Accordingly, MBP-immunoreactivity of the MBPh-immunoreactive particles was much stronger than that of the MBPh-immunoreactive myelinated nerve fibers (FIGURE 1A). Hence, we could

clearly distinguish the particles from the myelinated nerve fibers by using the anti-MBPh antibody in the present study.

MBP-immunoreactivity of the myelinated nerve fibers in the rat optic nerve visualized by using the anti-MBPh antibody was weaker than that in the monkey one (FIGURES 7A-E, 10B). In addition, pig and chicken MBP do not react with the anti-MBPh antibody and guinea pig MBP has slight reactivity with the antibody (Manufacturer's technical information). Thus, weak MBP-immunoreactivity of the rat myelinated nerve fibers visualized by using the anti-MBPh antibody is attributable to species differences in reactivity of the anti-MBPh antibody between for the rat MBP protein and for the monkey one.

Another underlying cause of a difference in MBPh-immunoreactivity between the particles and the myelinated nerve fibers is attributable to a dissimilarity in the density of the antigen, the MBP protein, each structure contains. The greater part of the myelin debris-like MBPh-immunoreactive particles is considered to be comprised of broken-myelin sheaths (See 4.8). Accordingly, the particles are MBP rich structure. However, the myelinated nerve fibers are not so rich in MBP, since the cross-sectional area of the myelin sheath occupied about 40% of the cross-sectional area overall in the myelinated nerve fiber of the rat optic nerve (see footnote[3]). This evidence provides an estimate that density of MBP antigen in the MBPh-immunoreactive myelinated nerve fibers was less than half of that in the MBPh-

[3] Forrester and Peters (1967) measured diameters of myelinated nerve fibers of the albino rat optic nerve. The modal diameter overall is 0.9 μm. The modal diameter excluding the myelin sheath is 0.7 μm. Based on this evidence, the author calculated the following values of a myelinated nerve fiber: cross-sectional area of the myelin sheath was 0.2512 μm^2 (39.51%); cross-sectional area excluding the myelin sheath was (0.35 X 0.35 X 3.14 =) 0.38465 μm^2 (60.49%); cross-sectional area overall was (0.45 X 0.45 X 3.14 =) 0.63585 μm^2 (100.00%).

immunoreactive particles. Hence, the weaker MBPh-immunoreactivity in the myelinated nerve fibers is attributed to the lower density of the antigen, the MBP protein, in the fibers.

4.3 | Comparison with previous findings

MBP-immunoreactive myelin sheaths have been described in the myelinated region of the rodent optic nerve by several research groups (Dixon and Eng, 1982; Marcos and Chan-Ling, 2000; Sun et al., 2009). In the present study, we have confirmed these observations. In addition, we have demonstrated the concentration of MBPh-immunoreactive particles in the distal-most part of the myelinated region in the normal rat optic nerve. Few studies have reported the concentration. Thus, the present study provides new evidence for myelin sheath morphology in the normal rat optic nerve.

4.4 | Colocalization of neural and glial proteins in the MBPh-immunoreactive particles

In the distal-most part of the myelinated region, bundles of myelinated nerve fiber interdigitate with columns of GFAP-immunoreactive cells. In addition, GFAP-immunoreactive filaments are aligned parallel to the optic nerve axis and distribute among myelinated nerve fiber bundles (Morcos and Chan-Ling, 2000; Kawano, 2015b). In the present study, the MBPh-immunoreactive particles were observed in the distal-most part, and were similar to the MBPh-immunoreactive myelin debris in the damaged-optic nerve of the glaucoma rat (present study, see DISCUSSION 4.6). It is reasonable to speculate that GFAP-immunoreactivity in the MBPh-immunoreactive particles is attributable to the GFAP-immunoreactive filaments located on or around myelinated nerve fibers since the particles were comprised of broken-myelin sheaths.

Myelin sheaths are parts of oligodendrocytes (Peters et al., 1990; Bron et al., 1997), and 97 % of GS-immunoreactive cells are oligodendrocytes (Kawano, 2015b). In addition, GS-immunoreactive fibers extend longitudinally along the long axis of the rat optic nerve, and are RIP-immunoreactive (Kawano, 2015b). This evidence indicates that the myelin sheaths contain GS, since RIP is a marker of oligodendrocytes including the myelin sheaths (Friedman et al., 1989). It is reasonable to consider that GS-immunoreactivity in the MBPh-immunoreactive particles attributes to GS in the myelin sheaths since the particles consisted of broken-myelin sheaths.

NF200-immunoreactive filaments were distributed in axons of optic nerve neurons (Peters et al., 1990; present study). It is reasonable to speculate that NS200-immunoreactivity in the MBPh-immunoreactive particles is attributable to NS200 distributed in the axons. The particles probably involve parts of broken-axons, since the particles were composed of broken-myelin sheaths which had insulated the broken-axons.

4.5 | Majority of MBPh-immunoreactive particles were isolated from Iba1-immunoreactive microglia in the normal rat optic nerve.

In the peripheral nervous system, transection of a peripheral nerve leads to a prompt recruitment of hematogenous macrophages (Perry et al., 1987; Stoll et al., 1989a; Brück, 1997; Stoll and Jander, 1999). These macrophages migrate to degenerating nerve fibers and adheres to myelin ovoids containing myelin debris (Stoll et al., 1989a; Stoll and Jander, 1999). Myelin debris is almost completely cleared within the first 2 weeks (Stoll and Jander, 1999).

In the central nervous system, however, microglia are able to transform into large phagocytes and thereby removing myelin debris. After transection of the optic nerve or of fiber tracts in the spinal cord, there is an early transient period of microglial activation, but

the appearance of large phagocytes is delayed by many weeks (Perry et al., 1987; Stoll et al., 1989b; George and Griffin, 1994; Stoll and Jander, 1999). Therefore, prolonged persistence of myelin debris in degenerating fiber tracts of the central nervous system has been observed (Stoll and Jander, 1999; Weinger et al., 2011). This evidence suggests that the prolonged persistence of the MBPh-immunoreactive particles is possible in the normal rat optic nerve. Accordingly, isolation of the particles from Iba1-immunoreactive microglia is also possible, since there is little discrepancy between the isolation and the prolonged persistence of the MBP-immunoreactive particles.

4.6 | Neuroanatomical comparison between the MBPh-immunoreactive particles and the MBPh-immunoreactive myelin debris

The MBPh-immunoreactive particles in the normal rat optic nerve were morphologically similar to the MBPh-immunoreactive myelin debris in the damaged-optic nerve of the glaucoma rat. This notion is supported by following 3 facts. First, the size of the MBPh-immunoreactive particles was broadly similar to that of the MBPh-immunoreactive myelin debris (FIGURES 6-7). Second, all differences in the mean sizes (area and perimeter) and the mean shape descriptors (circularity, AR (aspect ratio), roundness, and solidity) between the particles and the myelin debris were less than 3 percents (present study). Third, mean circularity and mean roundness of the particles were significantly different from those of the myelin debris. Accordingly, only 2 out of 6 differences in the mean sizes and the mean shape descriptors between the particles and the myelin debris were statistically significant (FIGURE 8). Thus, subtle but significant difference between the particles and the myelin debris was detected in two mean shape descriptors: mean circularity and mean roundness. Based on these facts, it is extremely difficult to fall the particles and the myelin debris into separate categories. Therefore, it is possible to accept that the MBPh-immunoreactive

particles were morphologically similar to the MBPh-immunoreactive myelin debris. Probably, the particles were comprised of broken-myelin sheaths. This notion is supported by evidence that majority of MBPh-immunoreactive particles were distributed on myelinated nerve fibers in the normal rat optic nerve (present study). Accordingly, it is appropriate to describe the particles as myelin debris-like MBPh-immunoreactive particles.

4.7 | Distribution of MBPh-immunoreactive particles in the mouse, rat, and monkey optic nerves

Distribution of MBPh-immunoreactive particles was observed not only in the rat but also in the mouse and monkey optic nerves in their distal-most part (present study). These findings suggest that the distribution of MBPh-immunoreactive particles in the optic nerve is similar among various mammalian species.

4.8 | Underlying causes of the concentration of the MBPh-immunoreactive particles in the distal-most part of the myelinated region of the normal rat optic nerve

Underlying causes of the concentration are discussed thoroughly in the companion paper, Kawano (2025). In brief, GFAP and GS are abundantly distributed in the distal-most part of the myelinated region in the normal rat optic nerve (Kawano, 2025). Since astrogliosis is a fibrous proliferation of glial cells in injured areas of the central nervous system, abundant distribution of GFAP in the distal-most part suggests that this part might be under the mildly pathological condition (McAteer and Choudhury, 2009; Kawano, 2025). Since GS in oligodendrocytes is increased in chronic pathological conditions in mice and humans, abundant distribution of GS in the distal-most part indicates that this part is under the mildly pathological condition (Ben Haim et al., 2021; Kawano, 2025). It is possible that these

histopathological backgrounds in the distal-most part impair myelin sheaths, then myelin debris-like MBPh-immunoreactive particles are created.

4.9 | Contributions of the MBPh-immunoreactive particles to neurohistopathology in the future

The concentration of the MBPh-immunoreactive particles were observed in the distal-most part of the myelinated region in the normal rat optic nerve. These particles were morphologically similar to MBPh-immunoreactive myelin debris in the damaged-optic nerve of the glaucoma rat (present study, see DISCUSSION 4.6). Therefore, the damaged-optic nerve was under severe pathological condition. Density of MBPh-immunoreactive myelin debris in the damaged-optic nerve of the glaucoma rat was higher than that in the distal-most part in the normal rat (FIGURE 7). In addition, density of these particles in the distal-most part is the highest in the myelinated region of the normal rat (Kawano, 2025). Recently, the distal-most part of the myelinated region is considered to be under mildly pathological condition, however, the other part is under physiological condition (Kawano, 2025, see DISCUSSION 4.4-4.8). Thus, density of MBPh-immunoreactive particles and/or myelin debris varied according to histopathological conditions. Therefore, it is possible that MBPh-immunoreactive particles and/or of myelin debris can be used as histopathological biomarkers.

4.10 | Conclusion

In summary, we demonstrated the concentration of MBPh-immunoreactive particles in the distal-most part of the myelinated region in the normal rat optic nerve. The MBPh-immunoreactive particles contained the real myelin basic protein. The MBPh-immunoreactive particles were morphologically similar to the MBPh-immunoreactive myelin

debris in the damaged-optic nerve of the glaucoma rat. MBPh-immunoreactive particles were also observed in the distal-most part of the myelinated region in the mouse and monkey optic nerves.

These results demonstrate that the myelin debris-like MBPh-immunoreactive particles are concentrated on the distal-most part of the myelinated region. This evidence indicates that the distal-most part is under mildly pathological condition. The evidence may provide clues as to the pathophysiological background that induces localized vulnerability of the myelin sheaths. Furthermore, it is possible that MBPh-immunoreactive particles and/or myelin debris can be used as the histopathological biomarkers, since density of MBPh-immunoreactive particles and/or myelin debris vary according to histopathological conditions (present study, see DISCUSSION 4.9).

Author Contributions

J.K.: Concept, Funding, Supervision, Investigation, Data analysis, Writing original draft, Writing – review and editing.

Acknowledgments

The author thanks Doctor Shiro Nakagawa (Professor Emeritus, Kagoshima University Graduate School of Medical and Dental Sciences) for providing the monkey eyes and optic nerves, Professor Masahisa Horiuchi (Department of Hygiene and Health Promotion Medicine, Kagoshima University Graduate School of Medical and Dental Sciences) for his expert advice on statistical analyses, and Associate Professor Kentaro Setoyama (Division of Laboratory Animal Resources and Research, Center for Advanced Science Research and

Promotion, Kagoshima University) for his expert advice on glaucoma rat management. This work was supported by an annual fund from Kagoshima University.

Conflicts of Interest

The author declares no conflicts of interest.

Data Availability Statement

The data that support the findings of this study are available from the corresponding author upon reasonable request.

REFERENCES

Balaratnasingam, C., Morgan, W. H., Johnstone, V., Cringle, S. J., & Yu, D. Y. (2009). Heterogeneous distribution of axonal cytoskeleton proteins in the human optic nerve. *Investigative ophthalmology & visual science, 50*(6), 2824-2838. https://doi.org/10.1167/iovs.08-3206

Ben Haim, L., Schirmer, L., Zulji, A., Sabeur, K., Tiret, B., Ribon, M., Chang, S., Lamers, W. H., Boillée, S., Chaumeil, M. M., & Rowitch, D. H. (2021). Evidence for glutamine synthetase function in mouse spinal cord oligodendrocytes. *Glia, 69*(12), 2812-2827. https://doi.org/10.1002/glia.24071

Benvegnù, S., Poggiolini, I., & Legname, G. (2010). Neurodevelopmental expression and localization of the cellular prion protein in the central nervous system of the mouse. *The Journal of Comparative Neurology, 518*(11), 1879-1891. https://doi.org/10.1002/cne.22357

Black, J. A., Waxman, S. G., & Hildebrand, C. (1985). Axo-glial relations in the retina-optic nerve junction of the adult rat: freeze-fracture observations on axon membrane structure. *Journal of Neurocytology, 14*(6), 887-907. https://doi.org/10.1007/BF01224803

Bosco, A., Inman, D. M., Steele, M. R., Wu, G., Soto, I., Marsh-Armstrong, N., Hubbard, W. C., Calkins, D. J., Horner, P. J., & Vetter, M. L. (2008). Reduced retina microglial activation and improved optic nerve integrity with minocycline treatment in the DBA/2J mouse model of glaucoma. *Investigative ophthalmology & visual science, 49*(4), 1437-1446. https://doi.org/10.1167/iovs.07-1337

Bosco, A., Steele, M. R., & Vetter, M. L. (2011). Early microglia activation in a mouse model of chronic glaucoma. *The Journal of Comparative Neurology, 519*(4), 599-620. https://doi.org/10.1002/cne.22516

Bron, A. J., Tripathi, R. C., & Tripathi, B. J. (1997). The Visual Pathway. In: A. J. Bron, R. C. Tripathi, & B. J. Tripathi (Eds.), *Wolff's Anatomy of the Eye and Orbit.* (8th ed., pp. 489-596). London: Chapman & Hall.

Brück, W. (1997). The role of macrophages in Wallerian degeneration. *Brain Pathology, 7*(2), 741-752. https://doi.org/10.1111/j.1750-3639.1997.tb01060.x

Butt, A. M. (2013). Structure and function of oligodendrocytes. In H. Kettenmann & B. R. Ransom (Eds.), *Neuroglia* (3rd ed., pp. 62-73). New York: Oxford University Press.

Butt, A. M., & Ransom, B. R. (1993). Morphology of astrocytes and oligodendrocytes during development in the intact rat optic nerve. *The Journal of Comparative Neurology, 338*(1), 141-158. https://doi.org/10.1002/cne.903380110

Chang, M. L., Wu, C. H., Jiang-Shieh, Y. F., Shieh, J. Y., & Wen, C. Y. (2007). Reactive changes of retinal astrocytes and Müller glial cells in kainate-induced neuroexcitotoxicity. *Journal of Anatomy, 210*(1), 54-65. https://doi.org/10.1111/j.1469-7580.2006.00671.x

Chen, M. S., Huber, A. B., van der Haar, M. E., Frank, M., Schnell, L., Spillmann, A. A., Christ, F., & Schwab, M. E. (2000). Nogo-A is a myelin-associated neurite outgrowth inhibitor and an antigen for monoclonal antibody IN-1. *Nature, 403*(6768), 434-439. https://doi.org/10.1038/35000219

Chrast, R., Saher, G., Nave, K. A., & Verheijen, M. H. (2011). Lipid metabolism in myelinating glial cells: lessons from human inherited disorders and mouse models. *Journal of Lipid Research, 52*(3), 419-434. https://doi.org/10.1194/jlr.R009761

Dixon, R. G., & Eng, L. F. (1982). Processing techniques for the demonstration of myelin basic protein in paraffin-embedded optic nerve: an immunoperoxidase study of the developing albino rat. *Journal of Histochemistry and Cytochemistry, 30*(3), 270-273. https://doi.org/10.1177/30.3.6174565

Dugas, J. C., Tai, Y. C., Speed, T. P., Ngai, J., & Barres, B. A. (2006). Functional genomic analysis of oligodendrocyte differentiation. *Journal of Neuroscience, 26*(43), 10967-10983. https://doi.org/10.1523/jneurosci.2572-06.2006

Duncan, I. D., & Radcliff, A. B. (2016). Inherited and acquired disorders of myelin: The underlying myelin pathology. *Experimental Neurology, 283*(Pt B), 452-475. https://doi.org/10.1016/j.expneurol.2016.04.002

Dyer, C. A., Kendler, A., Philibotte, T., Gardiner, P., Cruz, J., & Levy, H. L. (1996). Evidence for central nervous system glial cell plasticity in phenylketonuria. *Journal of Neuropathology & Experimental Neurology, 55*(7), 795-814. https://doi.org/10.1097/00005072-199607000-00005

Filbin, M. T. (2003). Myelin-associated inhibitors of axonal regeneration in the adult mammalian CNS. *Nat Rev Neurosci, 4*(9), 703-713. https://doi.org/10.1038/nrn1195

Forrester, J., & Peters, A. (1967). Nerve fibres in optic nerve of rat. *Nature, 214*(5085), 245-247. https://doi.org/10.1038/214245a0

Fox, J. (2017). *Using the R commander, A Point-and-Click Interface for R* (1st ed.). Boca Raton, Florida: Chapman and Hall/CRC Press. https://doi.org/10.1201/9781315380537

Friedman, B., Hockfield, S., Black, J. A., Woodruff, K. A., & Waxman, S. G. (1989). In situ demonstration of mature oligodendrocytes and their processes: An immunocytochemical study with a new monoclonal antibody, Rip. *Glia, 2*(5), 380-390. https://doi.org/10.1002/glia.440020510

Gaillard, F., Bonfield, S., Gilmour, G. S., Kuny, S., Mema, S. C., Martin, B. T., Smale, L., Crowder, N., Stell, W. K., & Sauvé, Y. (2008). Retinal anatomy and visual performance in a diurnal cone-rich laboratory rodent, the Nile grass rat (*Arvicanthis niloticus*). *The Journal of Comparative Neurology, 510*(5), 525-538. https://doi.org/10.1002/cne.21798

George, R., & Griffin, J. W. (1994). Delayed macrophage responses and myelin clearance during Wallerian degeneration in the central nervous system: the dorsal radiculotomy model. *Experimental Neurology, 129*(2), 225-236. https://doi.org/10.1006/exnr.1994.1164

Haverkamp, S., & Wässle, H. (2000). Immunocytochemical analysis of the mouse retina. *The Journal of Comparative Neurology, 424*(1), 1-23. https://doi.org/10.1002/1096-9861(20000814)424:1<1::AID-CNE1>3.0.CO;2-V

Hojo, M., Ohtsuka, T., Hashimoto, N., Gradwohl, G., Guillemot, F., & Kageyama, R. (2000). Glial cell fate specification modulated by the bHLH gene *Hes5* in mouse retina. *Development, 127*(12), 2515-2522. https://doi.org/10.1242/dev.127.12.2515

Howell, G. R., Libby, R. T., Jakobs, T. C., Smith, R. S., Phalan, F. C., Barter, J. W., Barbay, J. M., Marchant, J. K., Mahesh, N., Porciatti, V., Whitmore, A. V., Masland, R. H., & John, S. W. (2007). Axons of retinal ganglion cells are insulted in the optic nerve early in DBA/2J glaucoma. *Journal of Cell Biology, 179*(7), 1523-1537. https://doi.org/10.1083/jcb.200706181

Imai, Y., Ibata, I., Ito, D., Ohsawa, K., & Kohsaka, S. (1996). A novel gene iba1 in the major histocompatibility complex class III region encoding an EF hand protein expressed in a monocytic lineage. *Biochemical and Biophysical Research Communications, 224*(3), 855-862. https://doi.org/10.1006/bbrc.1996.1112

Ito, D., Tanaka, K., Suzuki, S., Dembo, T., & Fukuuchi, Y. (2001). Enhanced expression of Iba1, ionized calcium-binding adapter molecule 1, after transient focal cerebral ischemia in rat brain. *Stroke, 32*(5), 1208-1215. https://doi.org/10.1161/01.str.32.5.1208

Jeon, S. B., Yoon, H. J., Park, S. H., Kim, I. H., & Park, E. J. (2008). Sulfatide, a major lipid

component of myelin sheath, activates inflammatory responses as an endogenous stimulator in brain-resident immune cells. *Journal of Immunology, 181*(11), 8077-8087. https://doi.org/10.4049/jimmunol.181.11.8077

Johnson, E. C., Jia, L., Cepurna, W. O., Doser, T. A., & Morrison, J. C. (2007). Global changes in optic nerve head gene expression after exposure to elevated intraocular pressure in a rat glaucoma model. *Investigative ophthalmology & visual science, 48*(7), 3161-3177. https://doi.org/10.1167/iovs.06-1282

Ju, W. K., Misaka, T., Kushnareva, Y., Nakagomi, S., Agarwal, N., Kubo, Y., Lipton, S. A., & Bossy-Wetzel, E. (2005). OPA1 expression in the normal rat retina and optic nerve. *The Journal of Comparative Neurology, 488*(1), 1-10. https://doi.org/10.1002/cne.20586

Kanamori, A., Nakamura, M., Nakanishi, Y., Nagai, A., Mukuno, H., Yamada, Y., & Negi, A. (2004). Akt is activated via insulin/IGF-1 receptor in rat retina with episcleral vein cauterization. *Brain Research, 1022*(1-2), 195-204. https://doi.org/10.1016/j.brainres.2004.06.077

Kanda, Y. (2013). Investigation of the freely available easy-to-use software 'EZR' for medical statistics. *Bone Marrow Transplantation, 48*(3), 452-458. https://doi.org/10.1038/bmt.2012.244

Kawano, J. (2015a). Chemoarchitecture of glial fibrillary acidic protein (GFAP) and glutamine synthetase in the optic nerve of the monkey (*Macaca fuscata*): An immunohistochemical study. *Okajimas Folia Anatomica Japonica, 91*(4), 97-104. https://doi.org/10.2535/ofaj.91.97

Kawano, J. (2015b). Chemoarchitecture of glial fibrillary acidic protein (GFAP) and glutamine synthetase in the rat optic nerve: An immunohistochemical study. *Okajimas Folia Anatomica Japonica, 92*(1), 11-30. https://doi.org/10.2535/ofaj.92.11

Kawano, J. (2025). Heterogeneous distribution of glial cell proteins and of cell nucleus marker in the myelinated region of the normal rat optic nerve. *bioRxiv,* Submitted.

Kawano, J., Tanizawa, Y., & Shinoda, K. (2008). Wolfram syndrome 1 (*Wfs1*) gene expression in the normal mouse visual system. *The Journal of Comparative Neurology, 510*(1), 1-23. https://doi.org/10.1002/cne.21734

Kotter, M. R., Li, W. W., Zhao, C., & Franklin, R. J. (2006). Myelin impairs CNS remyelination by inhibiting oligodendrocyte precursor cell differentiation. *Journal of Neuroscience, 26*(1), 328-332. https://doi.org/10.1523/jneurosci.2615-05.2006

McAteer, M. A., & Choudhury, R. P. (2009). Applications of nanotechnology in molecular imaging of the brain. *Progress in Brain Research, 180*, 72-96. https://doi.org/10.1016/s0079-6123(08)80004-0

Melo, P., Moreno, V. Z., Vázquez, S. P., Pinazo-Durán, M. D., & Tavares, M. A. (2006). Myelination changes in the rat optic nerve after prenatal exposure to methamphetamine. *Brain Research, 1106*(1), 21-29. https://doi.org/10.1016/j.brainres.2006.05.020

Messam, C., Hou, J., Janabi, N., Monaco, M., Gravell, M., & Major, E. (2002). Glial cell types. In V. S. Ramachandran (Ed.), *Encyclopedia of the Human Brain* (1st ed., Vol. 2, pp. 369-387). San Diego: Academic Press. https://doi.org/10.1016/B0-12-227210-2/00152-7

Morcos, Y., & Chan-Ling, T. (2000). Concentration of astrocytic filaments at the retinal optic nerve junction is coincident with the absence of intra-retinal myelination: comparative and developmental evidence. *Journal of Neurocytology, 29*(9), 665-678. https://doi.org/10.1023/A:1010835404754

Naka, M., Kanamori, A., Negi, A., & Nakamura, M. (2010). Reduced expression of aquaporin-9 in rat optic nerve head and retina following elevated intraocular pressure.

Investigative ophthalmology & visual science, 51(9), 4618-4626. https://doi.org/10.1167/iovs.09-4712

Naskar, R., Wissing, M., & Thanos, S. (2002). Detection of early neuron degeneration and accompanying microglial responses in the retina of a rat model of glaucoma. *Investigative ophthalmology & visual science, 43*(9), 2962-2968.

Perry, V. H., Brown, M. C., & Gordon, S. (1987). The macrophage response to central and peripheral nerve injury. A possible role for macrophages in regeneration. *Journal of Experimental Medicine, 165*(4), 1218-1223. https://doi.org/10.1084/jem.165.4.1218

Peters, A., Palay, S. L., & Webster, H. d. (1991). *The Fine Structure of the Nervous System: Neurons and Their Supporting Cells* (3rd ed.). New York: Oxford University Press.

Riepe, R. E., & Norenburg, M. D. (1977). Müller cell localisation of glutamine synthetase in rat retina. *Nature, 268*(5621), 654-655. https://doi.org/10.1038/268654a0

Saari, J. C., Huang, J., Possin, D. E., Fariss, R. N., Leonard, J., Garwin, G. G., Crabb, J. W., & Milam, A. H. (1997). Cellular retinaldehyde-binding protein is expressed by oligodendrocytes in optic nerve and brain. *Glia, 21*(3), 259-268. https://doi.org/10.1002/(SICI)1098-1136(199711)21:3<259::AID-GLIA1>3.0.CO;2-0

Santos, A. M., Calvente, R., Tassi, M., Carrasco, M. C., Martín-Oliva, D., Martín -Teva, J. L., Navascués J., & Cuadros, M. A. (2008). Embryonic and postnatal development of microglial cells in the mouse retina. *The Journal of Comparative Neurology, 506*(2), 224-239. https://doi.org/10.1002/cne.21538

Saper, C. B. (2005). An open letter to our readers on the use of antibodies. *The Journal of Comparative Neurology, 493*(4), 477-478. https://doi.org/10.1002/cne.20839

Shareef, S. R., Garcia-Valenzuela, E., Salierno, A., Walsh, J., & Sharma, S. C. (1995). Chronic ocular hypertension following episcleral venous occlusion in rats. *Experimental Eye Research, 61*(3), 379-382. https://doi.org/10.1016/s0014-4835(05)80131-9

Smith, S. B., Brodjian, S., Desai, S., & Sarthy, V. (1997). Glial fibrillary acidic protein (GFAP) is synthesized in the early stages of the photoreceptor cell degeneration of the mi^{vit}/mi^{vit} (vitiligo) mouse. *Experimental Eye Research, 64*(4), 645-650. https://doi.org/10.1006/exer.1996.0249

Stoll, G., & Jander, S. (1999). The role of microglia and macrophages in the pathophysiology of the CNS. *Progress in Neurobiology, 58*(3), 233-247. https://doi.org/10.1016/s0301-0082(98)00083-5

Stoll, G., Griffin, J. W., Li, C. Y., & Trapp, B. D. (1989a). Wallerian degeneration in the peripheral nervous system: participation of both Schwann cells and macrophages in myelin degradation. *Journal of Neurocytology, 18*(5), 671-683. https://doi.org/10.1007/bf01187086

Stoll, G., Trapp, B. D., & Griffin, J. W. (1989b). Macrophage function during Wallerian degeneration of rat optic nerve: clearance of degenerating myelin and Ia expression. *Journal of Neuroscience, 9*(7), 2327-2335. https://doi.org/10.1523/jneurosci.09-07-02327.1989

Sun, D., Lye-Barthel, M., Masland, R. H., & Jakobs, T. C. (2009). The Morphology and Spatial Arrangement of Astrocytes in the Optic Nerve Head of the Mouse. *The Journal of Comparative Neurology, 516*(1), 1-19. https://doi.org/10.1002/cne.22058

Sun, X., Wang, X., Chen, T., Li, T., Cao, K., Lu, A., Chen, Y., Sun, D., Luo, J., Fan, J., Young, W., & Ren, Y. (2010). Myelin activates FAK/Akt/NF-kappaB pathways and provokes CR3-dependent inflammatory response in murine system. *PLoS One, 5*(2), e9380. https://doi.org/10.1371/journal.pone.0009380

Syed, Y. A., Zhao, C., Mahad, D., Möbius, W., Altmann, F., Foss, F., González, G. A., Sentürk, A., Acker-Palmer, A., Lubec, G., Lilley, K., Franklin, R. J. M., Nave, K. A.,

& Kotter, M. R. N. (2016). Antibody-mediated neutralization of myelin-associated EphrinB3 accelerates CNS remyelination. *Acta Neuropathologica, 131*(2), 281-298. doi:10.1007/s00401-015-1521-1

Talos, D. M., Fishman, R. E., Park, H., Folkerth, R. D., Follett, P. L., Volpe, J. J., & Jensen, F. E. (2006). Developmental regulation of alpha-amino-3-hydroxy-5-methyl-4-isoxazole-propionic acid receptor subunit expression in forebrain and relationship to regional susceptibility to hypoxic/ischemic injury. I. Rodent cerebral white matter and cortex. *The Journal of Comparative Neurology, 497*(1), 42-60. https://doi.org/10.1002/cne.20972

Wang, X., Cao, K., Sun, X., Chen, Y., Duan, Z., Sun, L., Guo, L., Bai, P., Sun, D., Fan, J., He, X., Young, W., & Ren, Y. (2015). Macrophages in spinal cord injury: phenotypic and functional change from exposure to myelin debris. *Glia, 63*(4), 635-651. https://doi.org/10.1002/glia.22774

Warr, W. B., de Olmos, J. S., & Heimer, L. (1981). Horseradish Peroxidase: The Basic Procedure. In L. Heimer & M. J. Robards (Eds.), *Neuroanatomical tract-tracing methods*. (1st ed., pp. 207-262). New York: Plenum Press.

Weinger, J. G., Brosnan, C. F., Loudig, O., Goldberg, M. F., Macian, F., Arnett, H. A., Prieto, A. L., Tsiperson, V., & Shafit-Zagardo, B. (2011). Loss of the receptor tyrosine kinase Axl leads to enhanced inflammation in the CNS and delayed removal of myelin debris during Experimental Autoimmune Encephalomyelitis. *Journal of Neuroinflammation, 8*, 49. https://doi.org/10.1186/1742-2094-8-49

Ye, H., & Hernandez, M. R. (1995). Heterogeneity of astrocytes in human optic nerve head. *The Journal of Comparative Neurology, 362*(4), 441-452. https://doi.org/10.1002/cne.903620402

Zabouri, N., Bouchard, J.-F., & Casanova, C. (2011). Cannabinoid receptor type 1 expression during postnatal development of the rat retina. *The Journal of Comparative Neurology, 519*(7), 1258-1280. https://doi.org/10.1002/cne.22534

Zhang, C., Guo, Y., Miller, N. R., & Bernstein, S. L. (2009). Optic nerve infarction and post-ischemic inflammation in the rodent model of anterior ischemic optic neuropathy (rAION). *Brain Research, 1264*, 67-75. https://doi.org/10.1016/j.brainres.2008.12.075

Zhou, T., Zheng, Y., Sun, L., Badea, S. R., Jin, Y., Liu, Y., Rolfe, A. J., Sun, H., Wang, X., Cheng, Z., Huang, Z., Zhao, N., Sun, X., Li, J., Fan, J., Lee, C., Megraw, T. L., Wu, W., Wang, G., & Ren, Y. (2019). Microvascular endothelial cells engulf myelin debris and promote macrophage recruitment and fibrosis after neural injury. *Nature Neuroscience, 22*(3), 421-435. https://doi.org/10.1038/s41593-018-0324-9

Figure Legends

FIGURE 1 A new (A) and a traditional (B) images of myelin basic protein (MBP) visualized by using fluorescent double immunohistochemistry in the myelinated region of the normal rat optic nerve. Both images show parts of longitudinal sections through the paramedian part. **A:** Considerable number of particles strongly labeled in magenta are distributed in the distal (anterior)-most part of the myelinated region. These particles and myelinated nerve fibers were labeled with a mouse monoclonal anti-human myelin basic protein (MBPh) antibody (clone SMI-99; Covance, Princeton, NJ; Alexa Fluor 594 label; magenta). This antibody reacts with Ala-Ser-Asp-Tyr-Lys-Ser (ASDYKS) in position 131-136 of the classic human myelin basic protein. **B:** An adjacent optic nerve section of panel A was double-immunostained for myelin basic protein. Myelinated nerve fibers were labeled with a rat monoclonal anti-cow myelin basic protein (MBPc) antibody (clone 12; Abcam, Cambridge, United Kingdom; Alexa Fluor 594 label; magenta). This antibody reacts with Asp-Glu-Asn-Pro-Val-Val (DENPVV) in position 82-87 of the full length protein of the cow myelin basic protein. The arrows indicate particles strongly labeled in magenta. **A-B:** Glial cells, majority of them were oligodendrocytes (Kawano, 2015b), were immunostained with anti-glutamine synthetase (GS) antibody (Sigma-Aldrich, Saint Louis, Missouri, USA; Alexa Fluor 488 label; green). Cell nuclei were labeled with bisBenzimide (Hoechst 33258; blue). These two images were taken with an LSM 700 confocal microscope (Carl Zeiss, Jena, Germany). Note that the particles are concentrated on the distal-most part of the myelinated region in the normal rat optic nerve. Interestingly, large number of the particles are seen in panel A, however, small number of them are detected in similar part of the myelinated region in panel B. In addition, majority of the particles are distributed on MBP-immunoreactive myelinated nerve fibers (A, B). m, myelinated region; u, unmyelinated region. Scale bar = 100 µm in upper right of A for B.

FIGURE 2 Fluorescent double immunohistochemistry by using two monoclonal anti-myelin basic protein (MBP) antibodies that target amino acid sequence are different. Images show a small square region of a longitudinal section through the paramedian part in the distal (anterior)-most part of the myelinated region in the normal rat optic nerve. **A:** Particles were labeled with a mouse monoclonal anti-human myelin basic protein (MBPh) antibody (clone SMI-99; Covance, Princeton, NJ; Alexa Fluor 594 label; magenta in D). This antibody reacts with Ala-Ser-Asp-Tyr-Lys-Ser (ASDYKS) in position 131-136 of the classic human myelin basic protein. **B:** Particles and myelinated nerve fibers were labeled with a rat monoclonal anti-cow myelin basic protein (MBPc) antibody (clone 12; Abcam, Cambridge, United Kingdom; Alexa Fluor 488 label; green in D). This antibody reacts with Asp-Glu-Asn-Pro-Val-Val (DENPVV) in position 82-87 of the full length protein of the cow myelin basic protein. **C:** Cell nuclei labeled with bisBenzimide (Hoechst 33258; blue in D). **D:** A color overlay image of panels A-C. The arrowheads in panels A, B, and D indicate MBPh-immunoreactive particles also immunolabeled with the anti-MBPc antibody. These images were taken with an LSM 700 confocal microscope (Carl Zeiss, Jena, Germany). Note that majority of MBPh-immunoreactive particles are also immunolabeled with the anti-MBPc antibody that target amino acid sequence is different from that of the anti-MBPh antibody (D). These facts indicate that the anti-MBPh antibody was immunoreactive for the real myelin basic protein and that the MBPh-immunoreactive particles contained the real myelin basic protein. In addition, majority of the MBP-immunoreactive particles are distributed on MBPc-immunoreactive myelinated nerve fibers (D). m, myelinated region. Scale bar = 20 μm in upper right of D for A-C.

FIGURE 3 Images showing distribution of glial fibrillary acidic protein (GFAP) and of myelin basic protein-immunoreactive particles visualized by using fluorescent double immunohistochemistry. The images represent a small rectangle region of a longitudinal section through the paramedian part in the distal (anterior)-most part of the myelinated region in the normal rat optic nerve. Several particles strongly labeled in white (A) and in magenta (D) were labeled with a mouse monoclonal anti-human myelin basic protein (MBPh) antibody (clone SMI-99; Covance, Princeton, New Jersey, USA; Alexa Fluor 594 label). GFAP was labeled with an anti-GFAP antibody (Dako, Glostrup, Denmark; Alexa Fluor 488 label; B; green in D). Cell nuclei were labeled with bisBenzimide (Hoechst 33258; C; blue in D). The arrowheads indicate strongly MBPh-immunoreactive particles. These images were taken with an LSM 700 confocal microscope (Carl Zeiss, Jena, Germany). Note that moderate GFAP-immunoreactivity is observed in the MBPh-immunoreactive particles (see GFAP-immunoreactivity pointed by the arrowheads in B). m, myelinated region. Scale bar = 10 µm in upper right of D for A-C.

FIGURE 4 **A-D:** Images showing distribution of glutamine synthetase (GS) and of myelin basic protein-immunoreactive particles visualized by using fluorescent double immunohistochemistry. The images represent a small rectangle region of a longitudinal section through the paramedian part in the distal (anterior)-most part of the myelinated region in the normal rat optic nerve. Several particles colored in white (A) and in magenta (D) were labeled with a mouse monoclonal anti-human myelin basic protein (MBPh) antibody (clone SMI-99; Covance, Princeton, New Jersey, USA; Alexa Fluor 594 label). The GS protein was labeled with an anti-GS antibody (Sigma-Aldrich, Saint Louis, Missouri, USA; Alexa Fluor 488 label; B; green in D). Cell nuclei were labeled with bisBenzimide (Hoechst 33258; C; blue in D). The arrowheads indicate strongly-to-moderately MBPh-immunoreactive particles

(A-B, D). These images were taken with an LSM 700 confocal microscope (Carl Zeiss, Jena, Germany). Note that moderate GS-immunoreactivity is observed in the MBPh-immunoreactive particles (see GS-immunoreactivity pointed by the arrowheads in B).

E-H: Images showing distribution of the neurofilament 200-kDa heavy chain (NF200) protein and of MBPh-immunoreactive particles visualized by using fluorescent double immunohistochemistry. The images represent a small rectangle region of a longitudinal section through the paramedian part in the distal-most part of the myelinated region in the normal rat optic nerve. Several particles labeled in white (E) and in magenta (H) were labeled with the anti-MBPh antibody (Alexa Fluor 594 label). The NF200 protein was labeled with an anti-NF200 antibody (Sigma-Aldrich, Saint Louis, Missouri, USA; Alexa Fluor 488 label; F; green in H). Cell nuclei were labeled with bisBenzimide (Hoechst 33258; G; blue in H). The arrowheads indicate strongly MBPh-immunoreactive particles. These images were taken with an LSM 700 confocal microscope (Carl Zeiss, Jena, Germany). Note that weak-to-moderate NF200-immunoreactivity is observed in the MBPh-immunoreactive particles (see NF-200 immunoreactivity pointed by the arrowheads in F). m, myelinated region. Scale bar = 10 μm in upper right of D for A-C, and for E-H.

FIGURE 5 Images showing distribution of ionized calcium binding adapter molecule 1 (Iba1)-labeled microglia and of myelin basic protein-immunoreactive particles visualized by using fluorescent double immunohistochemistry. The images represent a small square region of a longitudinal section through the paramedian part in the distal (anterior)-most part of the myelinated region in the normal rat optic nerve. **A:** Particles were labeled with a mouse monoclonal anti-human myelin basic protein (MBPh) antibody (clone SMI-99; Covance, Princeton, NJ; Alexa Fluor 594 label; magenta in D). **B:** Microglia were labeled with a rabbit polyclonal anti-Iba1 antibody (Wako Pure Chemical Industries, Osaka, Japan;

Alexa Fluor 488 label; green in D). **C:** Cell nuclei were labeled with bisBenzimide (Hoechst 33258; blue in D). **D:** A color overlay image of panels A-C. The arrows in panels A, B, and D indicate MBPh-immunoreactive particles engulfed by an Iba1-labeled microglia. Insets are higher-magnification photomicrographs around these particles and microglia. These images were taken with an LSM 700 (A-D) or an LSM 900 (insets) confocal microscopes (Carl Zeiss, Jena, Germany). Note that majority of MBPh-immunoreactive particles are isolated from Iba1-labeled microglia (D). In addition, at least five MBPh-immunoreactive particles are engulfed in the Iba1-labeled microglia (insets of A, B, and D). m, myelinated region. Scale bar = 20 µm in lower right of D for A-C; 5 µm in lower right of inset of D for insets of A-C.

FIGURE 6 Images showing distribution of myelin basic protein-immunoreactive myelin debris and of glutamine synthetase (GS) in the glaucoma rat optic nerve visualized by using fluorescent double immunohistochemistry (case code: glaucoma rat 3). Panels A and B demonstrate the distribution of the myelin debris in the glaucomatous (left) optic nerve. Panels C and D represent myelin basic protein-immunoreactive particles in the contralateral (right) optic nerve. The images were taken from longitudinal sections through the paramedian part in the distal (anterior)-most part of the myelinated region in the optic nerves. Cell nuclei were labeled with bisBenzimide (Hoechst 33258; blue in B, D). The GS protein was labeled with an anti-GS antibody (Sigma-Aldrich, Saint Louis, Missouri, USA; Alexa Fluor 488 label; green in B, D). Particles colored in white (A, C) and in magenta (B, D) were labeled with a mouse monoclonal anti-human myelin basic protein (MBPh) antibody (clone SMI-99; Covance, Princeton, New Jersey, USA; Alexa Fluor 594 label). The arrows indicate MBPh-immunoreactive myelin debris in the glaucomatous optic nerve (A, B), and MBPh-immunoreactive particles in the contralateral optic nerve (C, D). These images were taken

with an LSM 700 confocal microscope (Carl Zeiss, Jena, Germany). Note that the size of MBPh-immunoreactive particles (C, D) is broadly similar to that of MBPh-immunoreactive myelin debris (A, B). m, myelinated region; u, unmyelinated region. Scale bar = 200 μm in lower right of D for A-C.

FIGURE 7 **A-H:** Images used for statistical analyses of differences in sizes and in shape descriptors between myelin basic protein (MBP)-immunoreactive particles in the distal (anterior)-most part of the myelinated region in the normal rat optic nerve (A-E) and MBP-immunoreactive myelin debris in the same part of damaged-optic nerves in the glaucoma rat (F-H). As for code “NR17L14” in A, “NR”, “17”, “L”, and “14” indicate “normal rat”, “case number 17”, “left optic nerve”, and “section number 14”, respectively. As for code “GR3L10”, “GR” represents “glaucoma rat”. The particles and the myelin debris were visualized by fluorescent immunohistochemistry using a mouse monoclonal anti-human myelin basic protein (MBPh) antibody (clone SMI-99; Covance, Princeton, NJ; Alexa Fluor 594 label). These images were taken with an LSM700 confocal microscope (Carl Zeiss, Jena, Germany). Note that the bottom of each image sets at the border between the unmyelinated and myelinated regions. In addition, each image of the optic nerve was split along the pia mater in order to cut the background off the measurement area. Scale bar = 250 μm in H for A-G.

I: The image shows the orientation of A-H.

FIGURE 8 Charts show area, perimeter, and shape descriptors (circularity, AR (aspect ratio), roundness, and solidity) of myelin basic protein (MBP)-immunoreactive particles in the normal rat (NR) and those of myelin debris in damaged-optic nerves of the glaucoma rat (GR). Images of the MBP-immunoreactive particles in the NR and those of the

MBP-immunoreactive myelin debris in the GR were taken in the distal (anterior)-most part of the myelinated region of the optic nerve as shown in FIGURE 7A-H. Since anti-human myelin basic protein (MBPh) antibody (clone SMI-99) was used to visualize the particles and the myelin debris, MBPh is described instead of MBP in the following. **A-D:** Data are expressed as mean ± SD (standard deviation; n = 5 rats/ NR group; n = 3 rats/ GR group). Results of two-sample t-tests are written above the charts. An asterisk (*) in C represents significant difference with P = 0.032 < 0.05. Each solid black circle in A, B, C, and D indicates mean area, mean perimeter, mean circularity, and mean AR of the MBPh-immunoreactive particles or those of MBPh-immunoreactive myelin debris in each experimental case, respectively. **A:** Mean area of MBPh-immunoreactive particles in the NR and that of MBPh-immunoreactive myelin debris in the GR; NR: mean ± SD = 4.562 ± 0.435; GR: mean ± SD = 4.657 ± 0.421. **B.** Mean perimeter; NR: mean ± SD = 7.425 ± 0.388; GR: mean ± SD = 7.617 ± 0.343. **C.** Mean circularity; NR: mean ± SD = 0.923 ± 0.009; GR: mean ± SD = 0.907 ± 0.003. **D.** Mean AR; NR: mean ± SD = 1.428 ± 0.039; GR: mean ± SD = 1.471 ± 0.011.

E-F: Data are expressed as box and whisker plots (n = 5 rats/ NR group; n = 3 rats/ GR group). Results of Mann-Whitney U tests are written above the charts. An asterisk (*) in E represents significant difference with P = 0.036 < 0.05. Each solid black circle in E, and in F indicates mean roundness, and mean solidity of the MBPh-immunoreactive particles or those of MBPh-immunoreactive myelin debris in each experimental case, respectively. The upper whisker indicates the maximum value and the lower one represents the minimum value. The thick horizontal line in the box shows the median. The upper and lower borders of the box indicate the interquartile range.

Note that mean circularity and mean roundness of MBPh-immunoreactive particles were significantly different from those of MBPh-immunoreactive myelin debris ($p < 0.05$).

Accordingly, only 2 out of 6 differences in sizes and shape descriptors between the particles and the myelin debris were statistically significant. NS, not significant.

FIGURE 9 Images showing distribution of myelin basic protein-immunoreactive particles in the myelinated region of the mouse optic nerve. The images represent distribution of glutamine synthetase (GS) and of the particles visualized by using fluorescent double immunohistochemistry. The images were taken from a longitudinal section through the paramedian part in the distal (anterior)-most part of the myelinated region in the normal mouse optic nerve. The particles colored in white (B) and in magenta (D) were labeled with a mouse monoclonal anti-human myelin basic protein (MBPh) antibody (clone SMI-99; Covance, Princeton, New Jersey, USA; Alexa Fluor 594 label). The GS protein was labeled with an anti-GS antibody (Sigma-Aldrich, Saint Louis, Missouri, USA; Alexa Fluor 488 label; C; green in D). Cell nuclei were labeled with bisBenzimide (Hoechst 33258; A; blue in D). The arrows indicate MBPh-immunoreactive particles distributed in the myelinated region of the mouse optic nerve (B, D). These images were taken with an LSM 700 confocal microscope (Carl Zeiss, Jena, Germany). Note that substantial number of MBPh-immunoreactive particles are distributed in the myelinated region of the mouse optic nerve. m (afs), myelinated region (astrocytic filament sparse region). u (afd), unmyelinated region (astrocytic filament dense region). Scale bar = 100 μm in lower right of D for A-C.

FIGURE 10 Images showing distribution of myelin basic protein-immunoreactive particles in the retrolaminar (myelinated) region of the optic nerve in the monkey (*Macaca fuscata*). The images represent distribution of glutamine synthetase (GS) and of the particles visualized by using fluorescent double immunohistochemistry. The images were taken from a longitudinal section through the paramedian part in the distal (anterior)-most part of the

retrolaminar region in the monkey optic nerve. The particles colored in white (B) and in magenta (D) were labeled with a mouse monoclonal anti-human myelin basic protein (MBPh) antibody (clone SMI-99; Covance, Princeton, New Jersey, USA; Alexa Fluor 594 label). The GS protein was labeled with an anti-GS antibody (Sigma-Aldrich, Saint Louis, Missouri, USA; Alexa Fluor 488 label; C; green in D). Cell nuclei were labeled with bisBenzimide (Hoechst 33258; A; blue in D). In the monkey, myelinated fibers are clearly labeled with the anti-MBPh antibody. The arrows indicate an MBPh-immunoreactive particle distributed in the retrolaminar region of the monkey optic nerve (B, D). These images were taken with an LSM 700 confocal microscope (Carl Zeiss, Jena, Germany). Note that substantial number of MBPh-immunoreactive particles are distributed in the retrolaminar region of the monkey optic nerve. LC, lamina cribrosa. RL, retrolaminar region. Scale bar = 100 µm in lower right of D for A-C.

SUPPLEMENTARY FIGURE 1

For upload: MBPc_MBPh_RK01ON2_4R_X20Z05_900_1L.psd

Images of fluorescent double immunohistochemistry on three serial optic nerve sections demonstrating undetectable cross-reactions between a mouse monoclonal primary antibody and a goat anti-rat secondary antibody (C), and between a rat monoclonal primary antibody and a goat anti-mouse secondary antibody (J). These two monoclonal primary antibodies used were anti-myelin basic protein (MBP) antibodies that target amino acid sequence are different. The three serial optic nerve sections are longitudinal ones through the paramedian part in the distal (anterior)-most part of the myelinated region in the normal rat optic nerve. In addition, panels A-D show the first section, panels E-H indicate the second one, and panels I-L demonstrate the third one of the three serial optic nerve sections. **A, E, I:** Cell nuclei labeled with bisBenzimide (Hoechst 33258; blue in D, H, and L). **B, F:** Particles and myelinated nerve fibers were labeled with the mouse monoclonal anti-human myelin basic protein (MBPh) antibody (clone SMI-99; Covance, Princeton, NJ; Alexa Fluor 594 label; magenta in D, and H). This antibody reacts with Ala-Ser-Asp-Tyr-Lys-Ser (ASDYKS) in position 131-136 of the classic human myelin basic protein. **C:** No primary antibody generated in the rat (rat monoclonal anti-MBPc antibody, see G, K) was applied. **D, H, L:** Panels D, H, and L are overlay images of panels A-C, E-G, and I-K, respectively. **J:** No primary antibody generated in the mouse (mouse monoclonal anti-MBPh antibody, see B, F) was applied. **G, K:** Particles and myelinated nerve fibers were labeled with the rat monoclonal anti-cow myelin basic protein (MBPc) antibody (clone 12; Abcam, Cambridge, United Kingdom; Alexa Fluor 488 label; green in H, and L). This antibody reacts with Asp-Glu-Asn-Pro-Val-Val (DENPVV) in position 82-87 of the full length protein of the cow myelin basic protein. These images were taken with an LSM 700 confocal microscope (Carl Zeiss, Jena, Germany). Note that cross-reactions are not detectable between the mouse

monoclonal anti-MBPh antibody and the Alexa Fluor 488 conjugated goat anti-rat secondary antibody (C), or between the rat monoclonal anti-MBPc antibody and the Alexa Fluor 594 conjugated goat anti-mouse secondary antibody (J). These facts indicate that the fluorescent double immunohistochemistry by using the mouse monoclonal anti-MBPh antibody and the rat monoclonal anti-MBPc antibody was not artificial but real. Accordingly, MBPh and MBPc double-immunoreactive particles visualized in FIGURE 2D were not false positive but real. m, myelinated region; u, unmyelinated region. Scale bar = 100 μm in lower right of L for A-K.

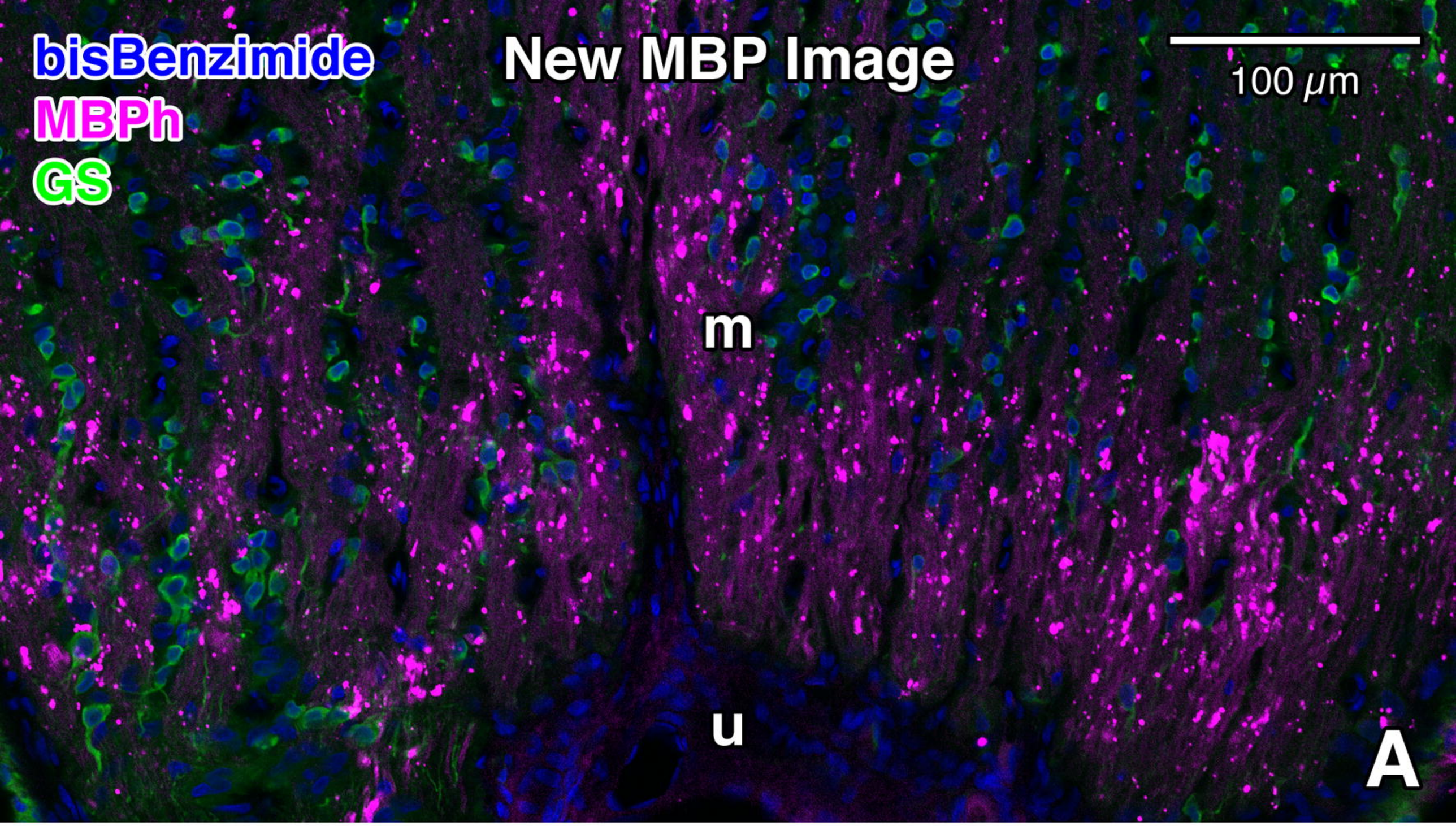
bisBenzimide
MBPh
GS
New MBP Image
100 μm
m
u
A

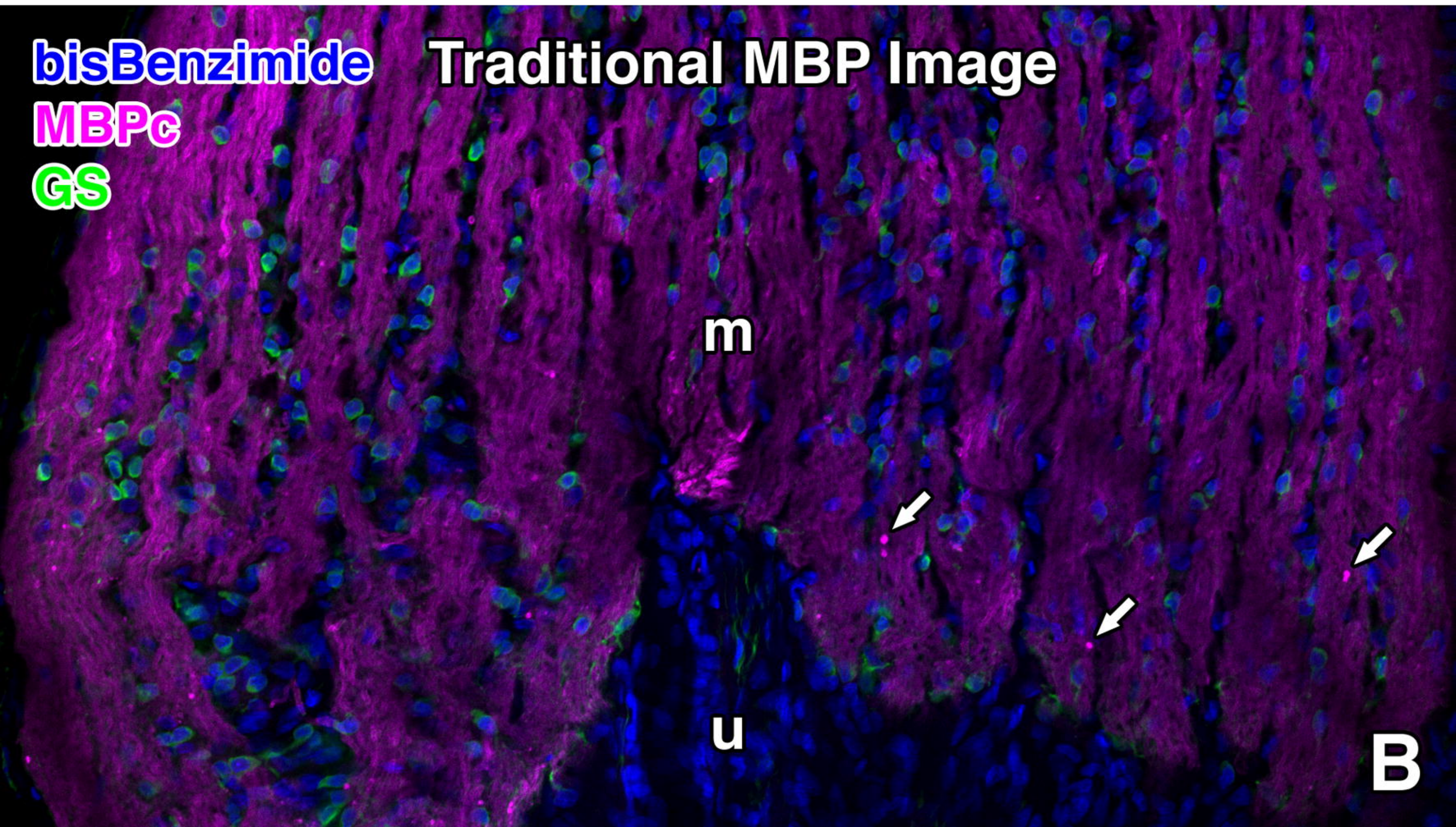
bisBenzimide
MBPc
GS
Traditional MBP Image
m
u
B

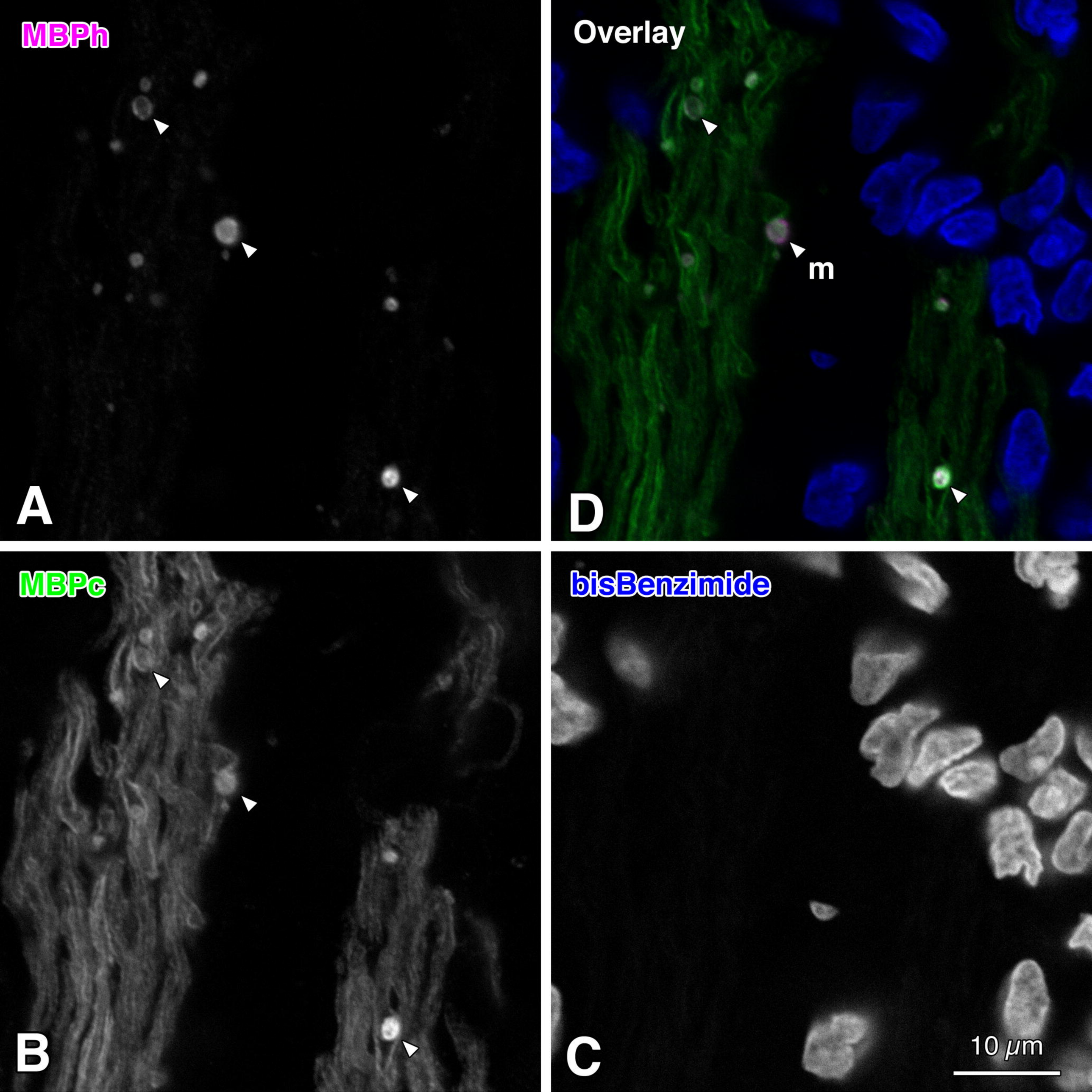
MBPh
A
MBPc
B
Overlay
m
D
bisBenzimide
C
10 μm

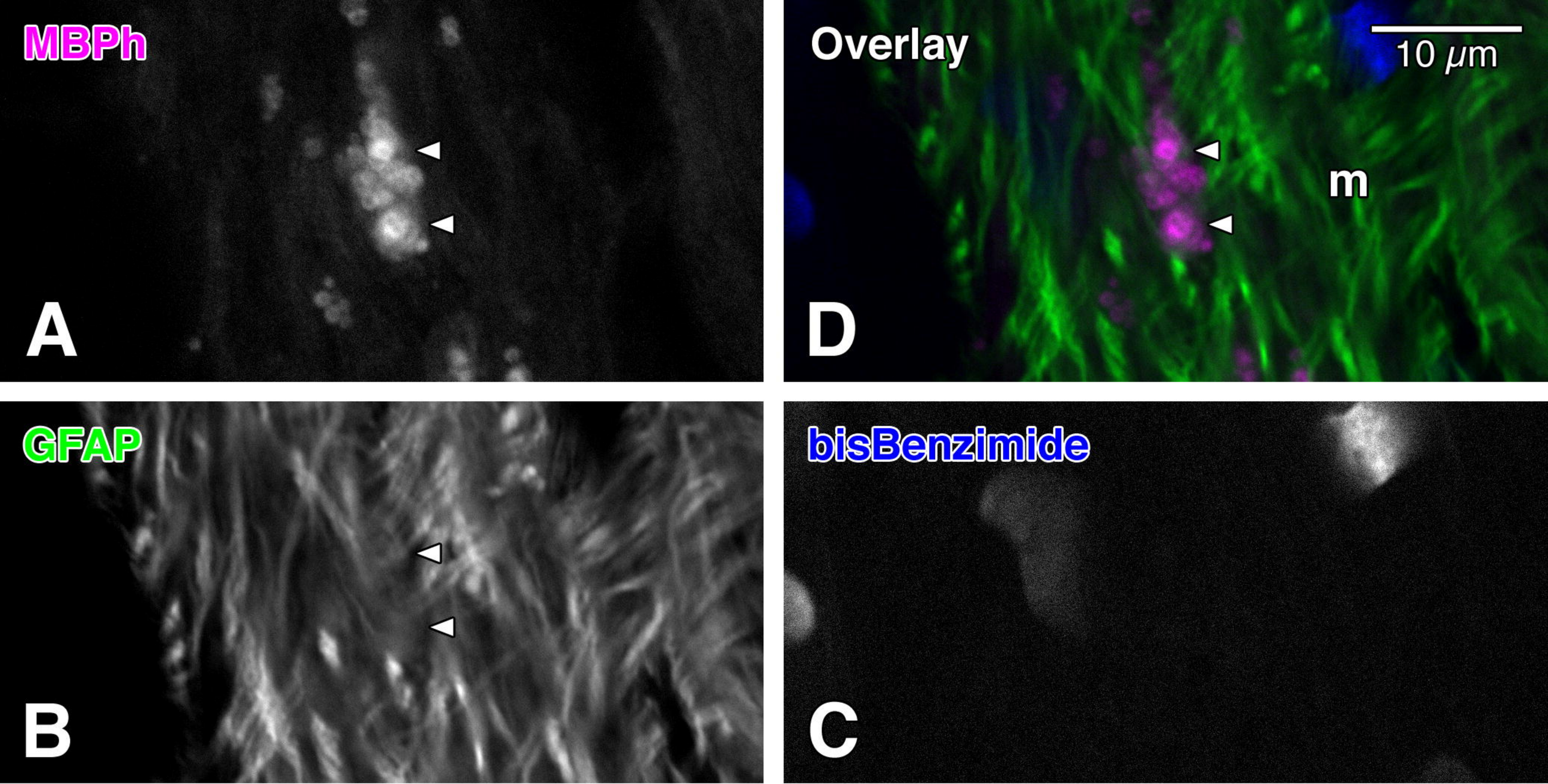
MBPh
A
Overlay
10 μm
m
D
GFAP
B
bisBenzimide
C

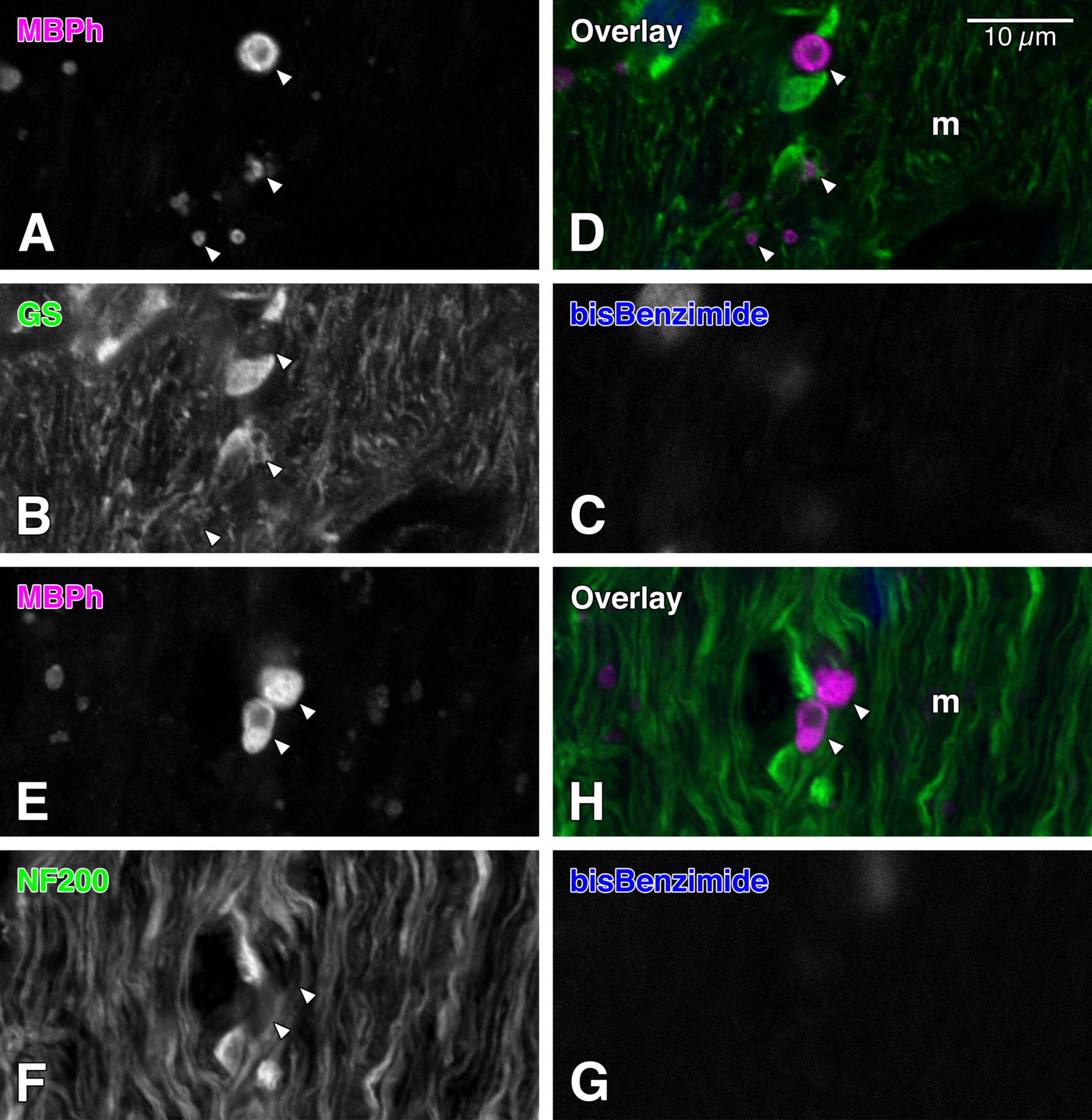
MBPh
A
Overlay
10 μm
m
D
GS
B
bisBenzimide
C
MBPh
E
Overlay
m
H
NF200
F
bisBenzimide
G

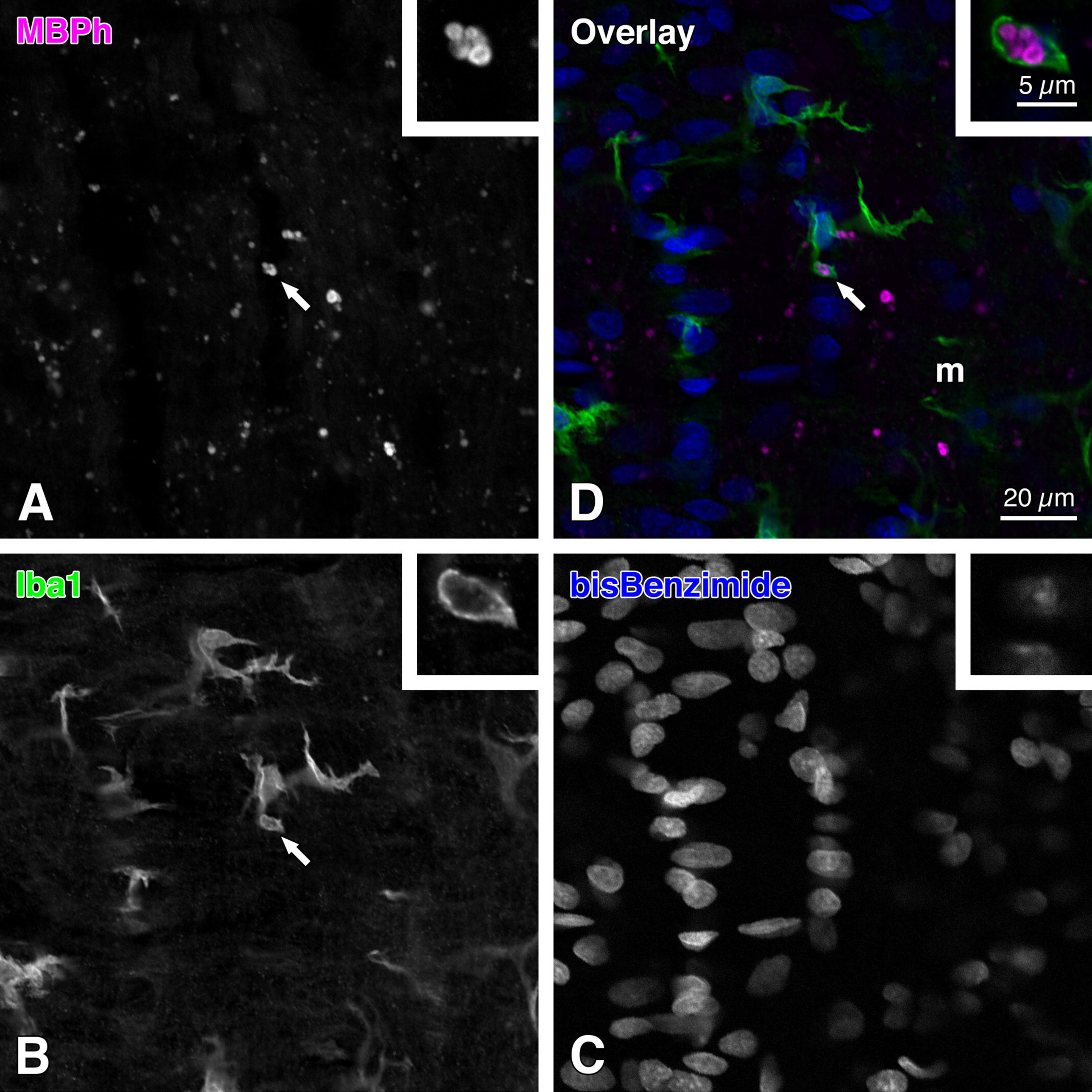
MBPh
A
Overlay
5 μm
m
D
20 μm
Iba1
B
bisBenzimide
C

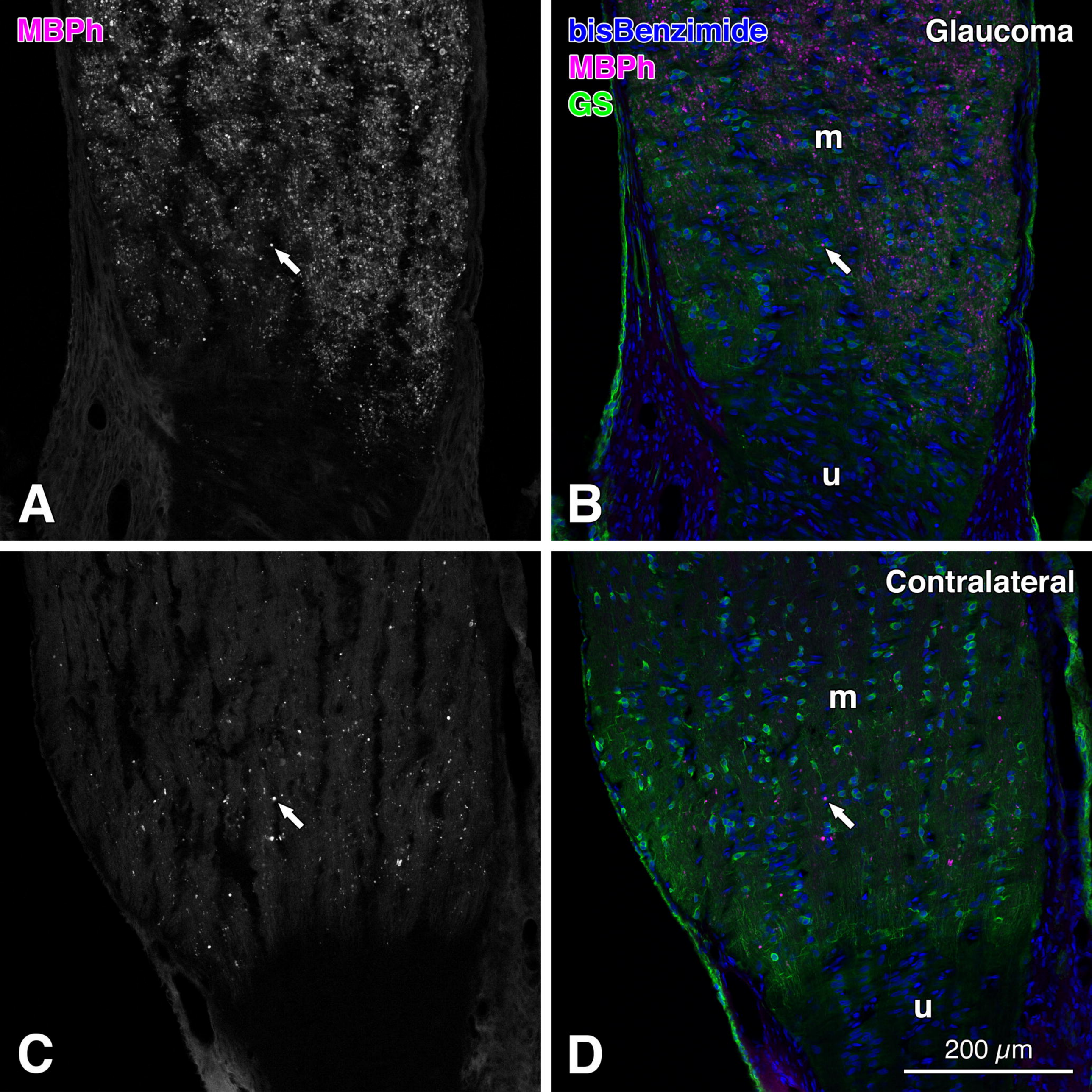
MBPh
A
bisBenzimide
MBPh
GS
Glaucoma
m
u
B
C
Contralateral
m
u
D
200 μm

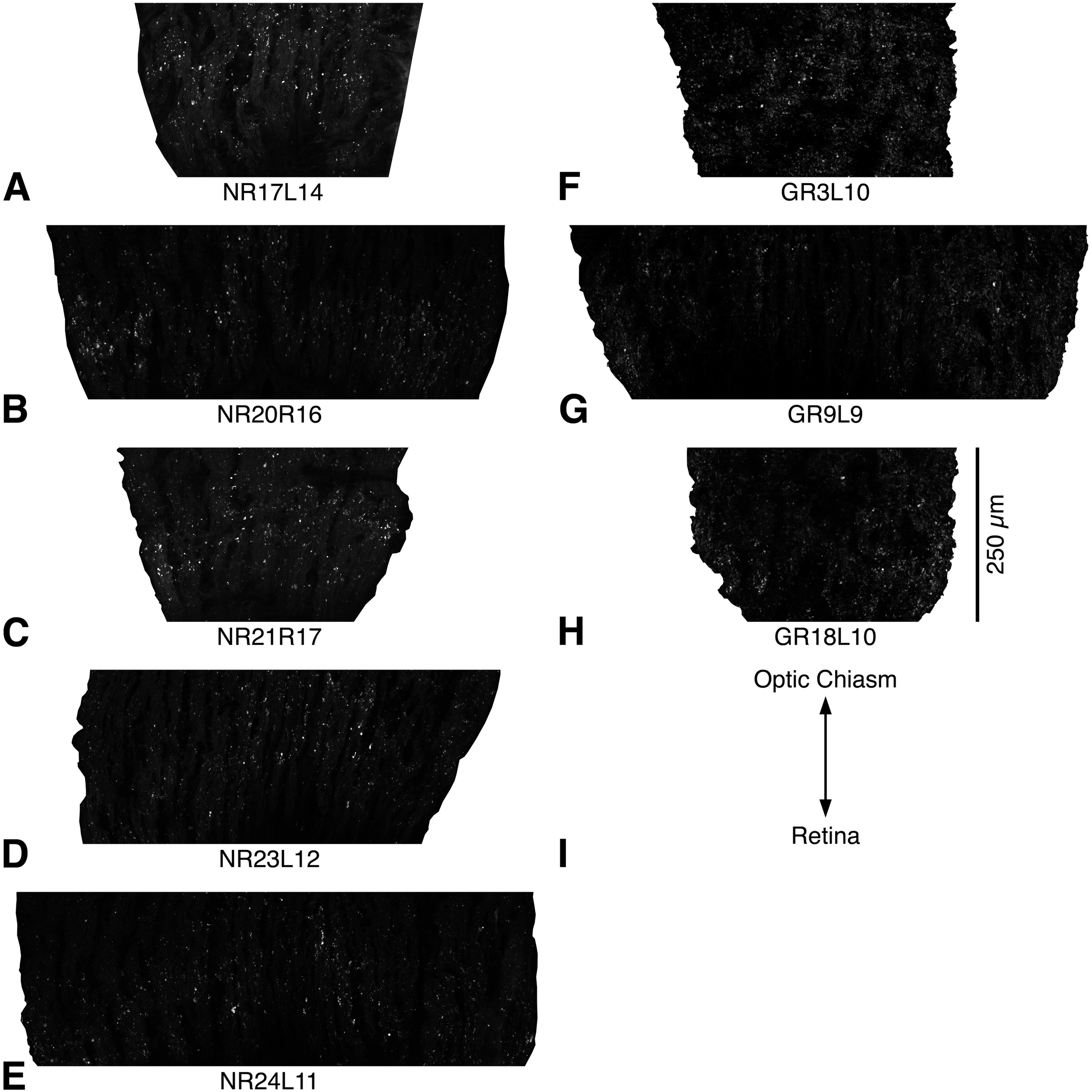
A
NR17L14
B
NR20R16
C
NR21R17
D
NR23L12
E
NR24L11
F
GR3L10
G
GR9L9
H
GR18L10
250 μm
Optic Chiasm
Retina
I

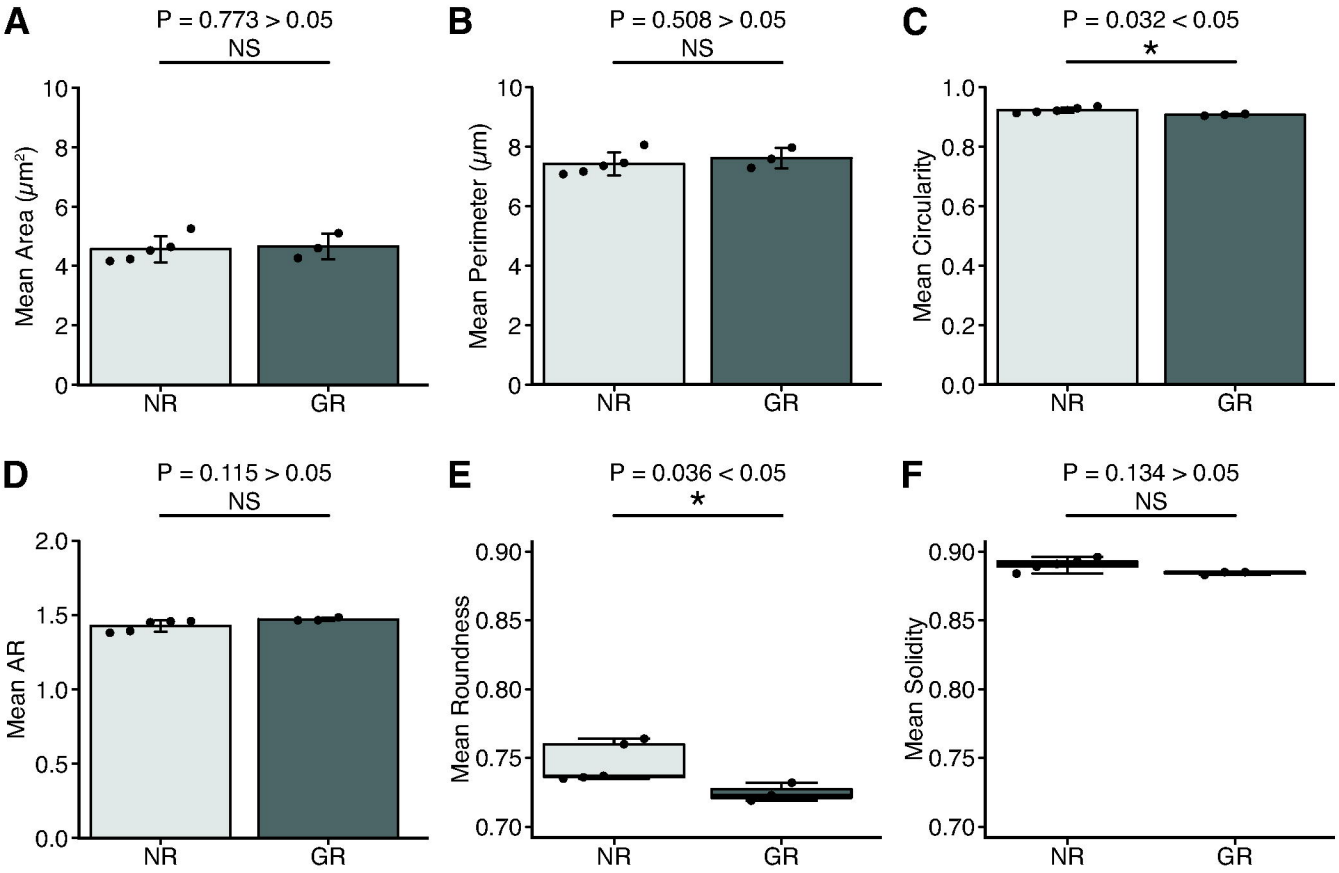
A
P = 0.773 > 0.05
NS
Mean Area (μm²)
0
2
4
6
8
10
NR
GR
B
P = 0.508 > 0.05
NS
Mean Perimeter (μm)
0
2
4
6
8
10
NR
GR
C
P = 0.032 < 0.05
*
Mean Circularity
0.0
0.2
0.4
0.6
0.8
1.0
NR
GR
D
P = 0.115 > 0.05
NS
Mean AR
0.0
0.5
1.0
1.5
2.0
NR
GR
E
P = 0.036 < 0.05
*
Mean Roundness
0.70
0.75
0.80
0.85
0.90
NR
GR
F
P = 0.134 > 0.05
NS
Mean Solidity
0.70
0.75
0.80
0.85
0.90
NR
GR

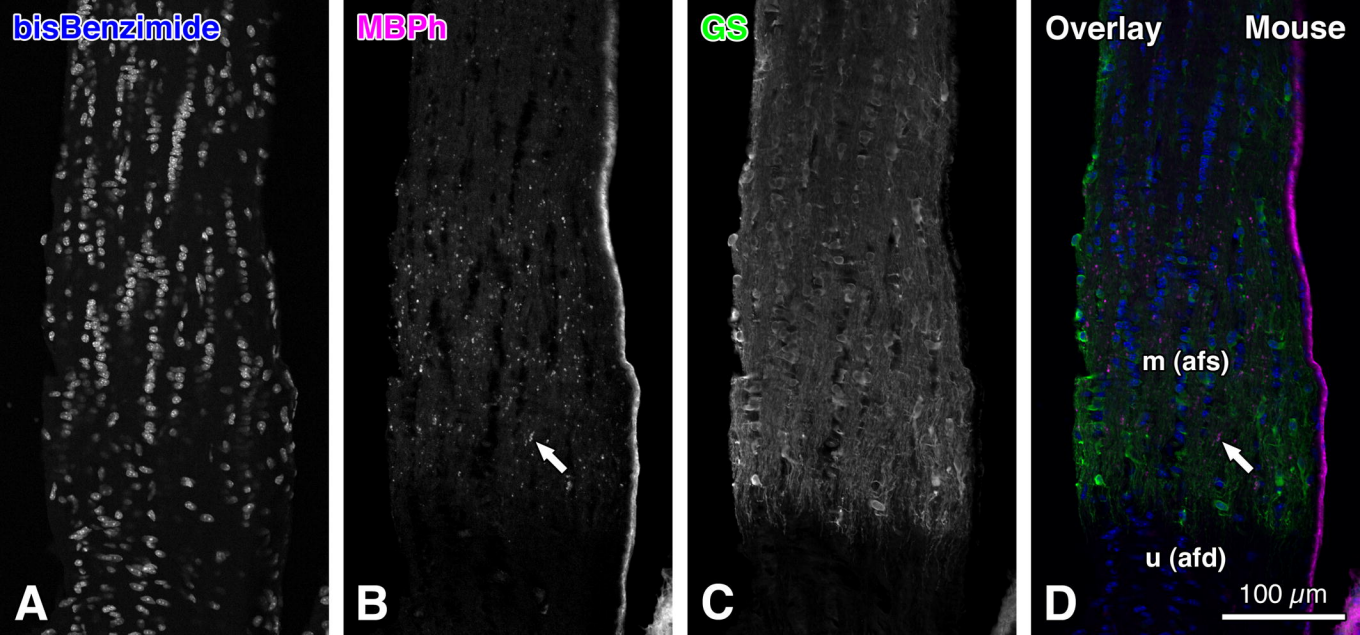
bisBenzimide
MBPh
GS
Overlay
Mouse
m (afs)
u (afd)
100 μm
A
B
C
D

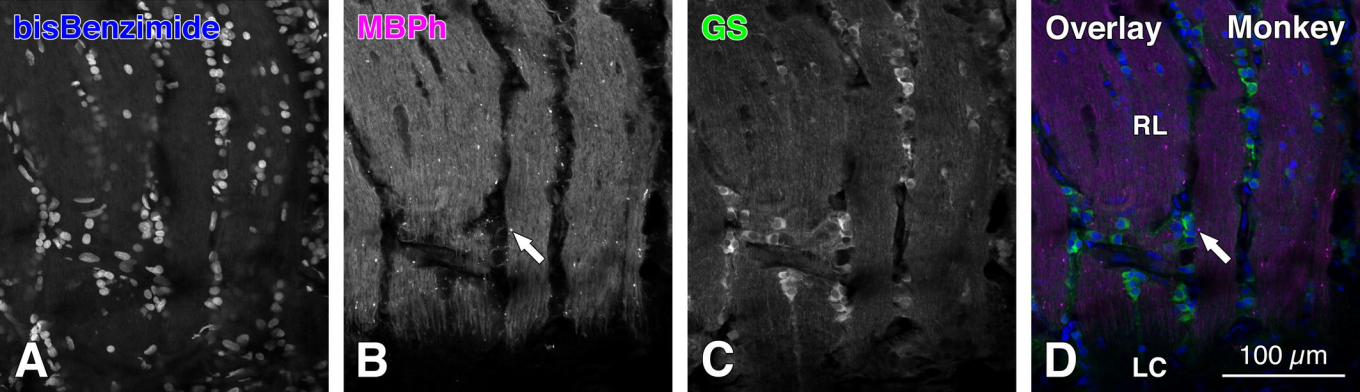
bisBenzimide
A
MBPh
B
GS
C
Overlay
Monkey
RL
D
LC
100 μm

TABLE 1. Primary antibodies used in this study.

Antigen	Immunogen	Manufacturer, cat. no., (lot no.)	Host, RRID	Dilution
Glial fibrillary acidic protein (GFAP)	GFAP isolated from the cow spinal cord	Dako (Glostrup, Denmark), Z0334, (00085136A)	Rb; polyclonal, RRID: AB_10013382	1:500
Glutamine synthetase (GS)	A synthetic peptide corresponding to the C-terminus of mouse glutamine synthetase (amino acids 357-373 with N-terminally added lysine) conjugated to KLH	Sigma-Aldrich (Saint Louis, MO), G2781, (115K4794)	Rb; polyclonal, RRID: AB_259853	1:5,000
Ionized calcium binding adaptor molecule 1 (Iba1)	A synthetic peptide corresponding C-terminus of Iba1	Wako (Osaka, Japan), 019-19741, (LAR4803)	Rb; polyclonal, RRID: AB_839504	1:1,000
Myelin basic protein, cow (MBPc) [clone 12]	Full length of the cow myelin basic protein	Abcam (Cambridge, United Kingdom), ab7349, (GR188102-12)	Rt; monoclonal, RRID: AB_305869	1:400
Myelin basic protein, human (MBPh) [SMI-99]	Human myelin basic protein peptide containing amino acids 131-136 (-Ala-Ser-Asp-Tyr-Lys-Ser-)	Covance (Princeton, NJ), SMI-99P, (E12DF00768)	Ms; monoclonal, RRID: AB_10120129	1:1,000
Neurofilament 200	Purified neurofilament 200 from the bovine spinal cord	Sigma-Aldrich, N4142, (059K4872)	Rb; polyclonal, RRID: AB_477272	1:100

Abbreviations: Ms, mouse; Rb, rabbit, Rt, rat..

TABLE 2. Comparison of mean sizes (area and perimeter) and mean shape descriptors (circularity, AR (aspect ratio), roundness, and solidity) of MBPh-immunoreactive particles in the normal rat (NR) optic nerve to those of MBPh-immunoreactive myelin debris in the damaged optic nerve of the glaucoma rat (GR).

	NR Measurements	GR Measurements	Ratio of NR Mean to GR Mean
Mean area	4.562 ± 0.435	4.657 ± 0.421	0.980
Mean perimeter	7.425 ± 0.388	7.617 ± 0.343	0.975
Mean circularity	0.923 ± 0.009	0.907 ± 0.003	1.018
Mean AR	1.428 ± 0.039	1.471 ± 0.011	0.971
Mean roundness	0.746 ± 0.014	0.725 ± 0.007	1.029
Mean solidity	0.891 ± 0.005	0.884 ± 0.001	1.008

Data are expressed as mean ± SD (standard deviation; n = 5 rats/ NR group; n = 3 rats/ GR group). Images used for this comparison are shown in FIGURE 7A-H. These images were taken in the distal (anterior)-most part of the myelinated region. The longitudinal length of each image was 250 µm. An abbreviation MBPh is described to indicate the myelin basic protein, since the monoclonal antibody against the human myelin basic protein (MBPh; clone SMI-99) was used to visualize the myelin basic protein.

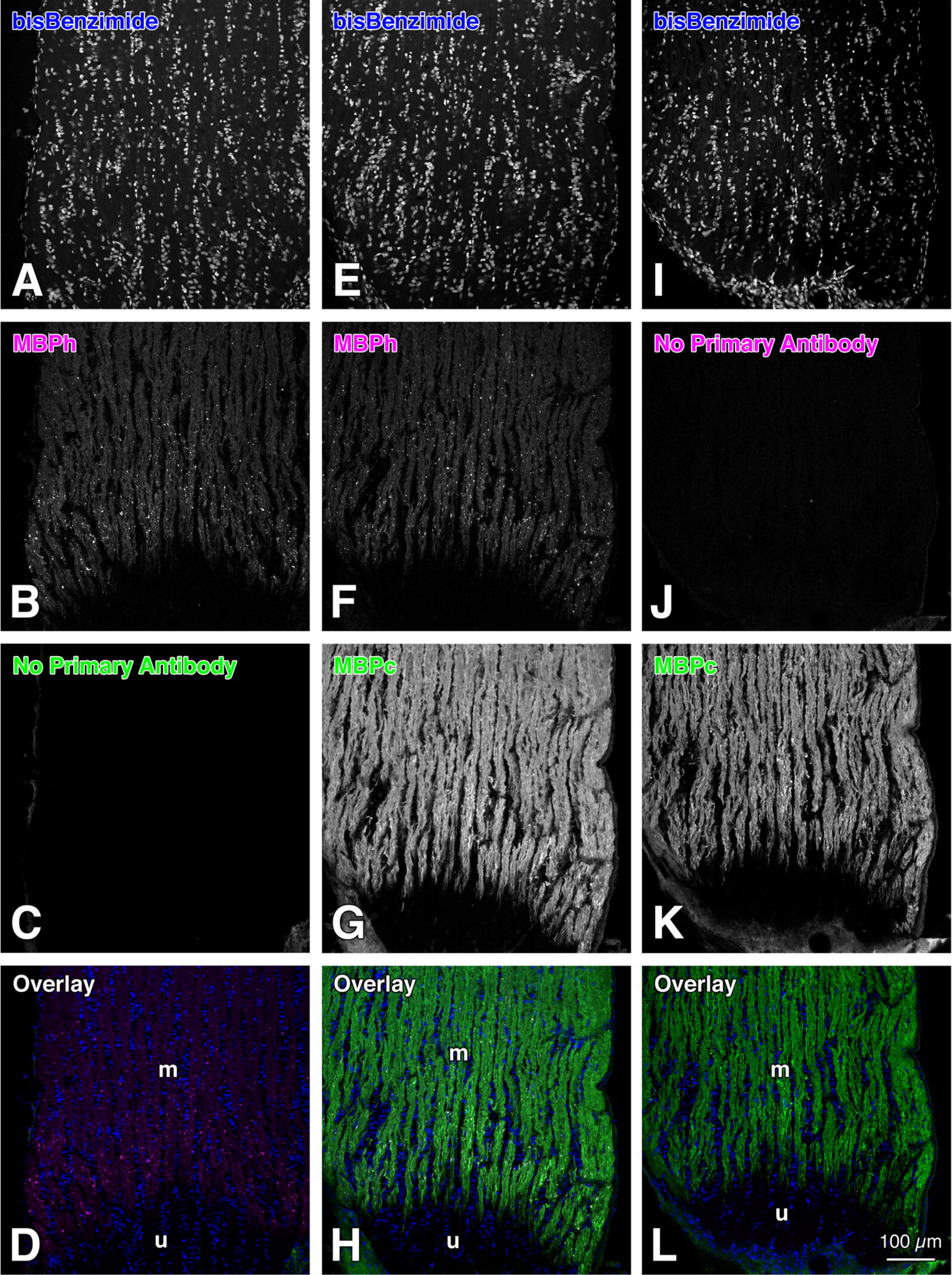
bisBenzimide
bisBenzimide
bisBenzimide
A
E
I
MBPh
MBPh
No Primary Antibody
B
F
J
No Primary Antibody
MBPc
MBPc
C
G
K
Overlay
Overlay
Overlay
m
m
m
u
u
u
D
H
L
100 μm